PB83-246082

Treatment of Gaseous Emissions from Steelplants Containing Small Concentrations of Hydrocarbon Vapors

Massachusetts Inst. of Tech., Cambridge

Prepared for

Industrial Environmental Research Lab.
Research Triangle Park, NC

Aug 83

U.S. Department of Commerce
National Technical Information Service
NTIS

PB83-246082

EPA-600/2-83-065
August 1983

TREATMENT OF GASEOUS EMISSIONS FROM STEELPLANTS CONTAINING SMALL CONCENTRATIONS OF HYDROCARBON VAPORS

by

H.X. Lambert and Julian Szekely
Department of Materials Science and Engineering
Massachusetts Institute of Technology
Cambridge, Massachusetts 02139

EPA Grant R806050

EPA Project Officer: John S. Ruppersberger

Industrial Environmental Research Laboratory
Industrial Processes Branch
Research Triangle Park, NC 27711

Prepared for

U.S. Environmental Protection Agency
Office of Research and Development
Washington, D.C. 20460

REPRODUCED BY
NATIONAL TECHNICAL
INFORMATION SERVICE
U.S. DEPARTMENT OF COMMERCE
SPRINGFIELD, VA. 22161

TECHNICAL REPORT DATA
(Please read Instructions on the reverse before completing)

1. REPORT NO.	2.	3. RECIPIENT'S ACCESSION NO.
EPA-600/2-83-065		PB83-246082

4. TITLE AND SUBTITLE	5. REPORT DATE
Treatment of Gaseous Emissions from Steelplants Containing Small Concentrations of Hydrocarbon Vapors	August 1983
	6. PERFORMING ORGANIZATION CODE
7. AUTHOR(S)	8. PERFORMING ORGANIZATION REPORT NO.
H.X. Lambert and Julian Szekely	
9. PERFORMING ORGANIZATION NAME AND ADDRESS	10. PROGRAM ELEMENT NO.
Department of Materials Science and Engineering Massachusetts Institute of Technology Cambridge, Massachusetts 02139	11. CONTRACT/GRANT NO. R806050
12. SPONSORING AGENCY NAME AND ADDRESS	13. TYPE OF REPORT AND PERIOD COVERED
EPA, Office of Research and Development Industrial Environmental Research Laboratory Research Triangle Park, NC 27711	Final; 9/78-4/83 14. SPONSORING AGENCY CODE EPA/600/13

15. SUPPLEMENTARY NOTES IERL-RTP project officer is John S. Ruppersberger, Mail Drop 63, 919/541-2733.

16. ABSTRACT The report gives results of an investigation of the feasibility of using a shallow fluidized bed of activated charcoal to remove small concentrations of hydrocarbon vapors in the presence of water vapor. This system can be applied to cleaning off-gases from sinterplants, coke ovens, and/or foundries. The investigated range of hydrocarbon vapors is 100-500 ng/cu cm air. It was found that a shallow fluidized bed of activated charcoal can efficienctly remove hydrocarbons in preference to moisture at 80 C. The overall mass transfer coefficient can be calculated from data obtained in a laboratory apparatus, and the influence of various parameters on the overall reaction rate is discussed. A mathematical model based on adsorption theory is presented, which provides a means for testing the validity of the assumptions and also for preliminary scale-up calculations.

17. KEY WORDS AND DOCUMENT ANALYSIS

a. DESCRIPTORS	b. IDENTIFIERS/OPEN ENDED TERMS	c. COSATI Field/Group
Pollution Sintering Iron and Steel Industry Hydrocarbons Coking Vapors Foundries Activated Carbon Fluidized Bed Processors Mathematical Models	Pollution Control Stationary Sources	13B 13H 05C, 11F 07C 07D 11G 131, 07A 12A

18. DISTRIBUTION STATEMENT	19. SECURITY CLASS (This Report)	21. NO. OF PAGES
Release to Public	Unclassified	120
	20. SECURITY CLASS (This page)	22. PRICE
	Unclassified	

EPA Form 2220-1 (9-73)

NOTICE

THIS DOCUMENT HAS BEEN REPRODUCED FROM THE BEST COPY FURNISHED US BY THE SPONSORING AGENCY. ALTHOUGH IT IS RECOGNIZED THAT CERTAIN PORTIONS ARE ILLEGIBLE, IT IS BEING RELEASED IN THE INTEREST OF MAKING AVAILABLE AS MUCH INFORMATION AS POSSIBLE.

NOTICE

This document has been reviewed in accordance with U.S. Environmental Protection Agency policy and approved for publication. Mention of trade names or commercial products does not constitute endorsement or recommendation for use.

ABSTRACT

In this research, the feasibility of using a shallow fluidized bed of activated charcoal, to remove small concentrations of hydrocarbon vapors in the presence of water vapor is investigated. This system can be applied to cleaning off-gases from sinterplants, coke ovens, and/or foundaries. The investigated range of hydrocarbon vapors is 100 to 500 ng/cm^3 air.

It is found that a shallow fluidized bed of activated charcoal can efficiently remove hydrocarbons in preference to moisture at 80°C. The overall mass transfer coefficient can be calculated from data obtained in a laboratory apparatus and the influence of various parameters on the overall reaction rate is discussed.

A mathematical model based on adsorption theory is presented, which provides a means for testing the validity of the assumptions and also for preliminary scale up calculations.

Reproduced from best available copy.

FOREWORD

This report is being published, despite its not complying with all EPA/ORD publication requirements, because of the worthwhile information it contains. Repeated attempts, over a period of years, have failed to produce an acceptable final report from the grantee. The cover, title page, foreword, and certain other administrative features normally associated with published EPA/ORD reports were provided by IERL-RTP to satisfy minimum reporting requirements.

Although the research described in this document has been funded in part by the U.S. EPA, it has not been subjected to the Agency's normally required peer review; therefore, it does not necessarily reflect the Agency's views and no official endorsement should be inferred.

TABLE OF CONTENTS

Chapter		Page
	ABSTRACT	iii
	Foreword	iii
	LIST OF FIGURES	ix
	LIST OF TABLES	xi
	ACKNOWLEDGEMENTS	xii
1	INTRODUCTION	1
	1.1 Setting of the problem	1
	1.2 Brief review of existing technologies	3
	1.3 Solution under investigation	3
2	LITERATURE SURVEY	5
	2.1 Physical adsorption	5
	2.1.1 Definitions	5
	2.1.2 Models of physical adsorption	6
	2.1.3 Adsorption of multi-component mixtures	9
	2.1.4 Influence of temperature on the adsorption reaction	10
	2.2 Fluidization	12
	2.2.1 Definitions	12
	2.2.2 Minimum fluidization velocity and terminal velocity	12
	2.2.3 Characterization of the particles	16
	2.2.4 Flow patterns	18
	2.2.4.1 Solid flow patterns	18
	2.2.4.2 Gas flow patterns	19

Preceding page blank

TABLE OF CONTENTS (Cont'd.)

Chapter		Page
	2.2.5 Bubbling in fluidized beds	20
	2.3 Activated charcoal	21
	2.4 Hydrocarbons	22
	2.5 Adsorption in fluidized beds; scale up	24
	2.6 Summary	26
3	APPARATUS AND EXPERIMENTAL METHOD	27
	3.1 Apparatus and experimental method	27
	3.1.1 Description of the apparatus	27
	3.1.2 Analytical gas chromatograph	27
	3.1.3 Description of an experiment	30
	3.1.4 Analysis of an experiment	33
	3.2 Parameters influencing the experiments	37
	3.2.1 Choice of the adsorbent	37
	3.2.2 Choice of the adsorbate	41
	3.2.3 Temperature of the bed	41
	3.2.4 Fluidization velocity	42
	3.2.5 Height of the bed, feed concentration, particle diameter	46
	3.3 Materials and specifications: setting of the parameters	46
	3.3.1 Materials and specifications	46
	3.3.2 Setting of the parameters	50

TABLE OF CONTENTS (Cont'd.)

Chapter		Page
4	RESULTS AND MATHEMATICAL MODEL	52
	4.1 Results	52
	4.1.1 Measurement of the isotherm	
	4.1.2 Analysis of a typical experiment	54
	4.1.3 Mass transfer coefficients	56
	4.1.3.1 Overall mass transfer coefficient assuming gas piston flow pattern	60
	4.1.3.2 Overall mass transfer coefficient assuming perfect gas backmixing	63
	4.1.4 Mass transfer correlations	63
	4.1.5 Comparison of the results	65
	4.2 Mathematical model	68
	4.2.1 Solid phase	71
	4.2.2 Gas phase	72
	4.3 Computer resolution of the mathematical modeling	74
	4.3.1 Method	74
	4.3.2 Development of the computer program	75
	4.4 Validity of the model	78
5	PRELIMINARY SCALE UP CALCULATIONS AND GENERAL CONCLUSIONS	82
	5.1 Scale up calculations	82
	5.1.1 Fugitive emissions	82
	5.1.2 Point source emissions	83
	5.2 General conclusions	85

TABLE OF CONTENTS (Cont'd.)

Chapter

REFERENCES 89

LIST OF SYMBOLS 93

APPENDICES 97

APPENDIX A Use of the AGC for the determination of the isotherm 98

APPENDIX B Computer listing 101

APPENDIX C Calibration 107

LIST OF FIGURES

Figure		Page
1-1	Sources of air pollution at integrated steelplant	2
2-1	Heat of adsorption of n-alkanes	11
2-2	Pressure drop-velocity relationship	13
2-3	Fraction of coke oven light oil	23
2-4	Sketch of the COURTAULDS process	25
3-1	Sketch of the apparatus	28
3-2	Sketch of the analytical gas chromatograph	31
3-3	Sketch of the micro-valve	32
3-4	Calibration of the gas chromatograph	34
3-5	Chromatogram	36
3-6	Adsorption of n-tetradecane on activated alumina	39
3-7	Adsorption of n-tetradecane on a deep bed of activated alumina	40
3-8	Effect of temperature on the uptake	44
3-9	N-tetradecane vapour pressure vs temperature	48
3-10	Charcoal pore size distribution	49
3-11	Sketch of the fluidized bed	51
4-1	80°C-isotherm of adsorption of n-tetradecane on activated charcoal	53
4-2	Typical adsorption run	55
4-3	Mass transfer controlling steps	57
4-4	Adsorption of n-tetradecane on shallow fluidized beds of activated charcoal	61
4-5	Plot of Re_p vs Sh and comparison with the results of other investigators	66

LIST OF FIGURES (Cont'd.)

Figure		Page
4-6	Adsorption of water on activated charcoal	69
4-7	Definition of the coordinates for mass balance establishment	70
4-8	Computer flow chart	77
4-9	Validity of the mathematical model: solid phase	79
4-10	Validity of the mathematical model: gas phase	80
5-1	Possible flow chart of the proposed system	86

LIST OF TABLES

Table		Page
3-1	Summary of results involving activated alumina, the air stream being saturated in moisture at room temperature.	38
3-2	Adsorption of hydrocarbon on activated charcoal	43
4-1	Mass transfer coefficients assuming perfect solid backmixing and gas piston flow pattern, at 0 coverage.	62
4-2	Mass transfer coefficients assuming perfect solid backmixing and perfect gas backmixing at zero coverage	64
4-3	Calculated Sherwood and Reynolds numbers assuming gas piston flow pattern, then complete gas mixing	67

ACKNOWLEDGEMENTS

The authors wish to express their thanks to the Environmental Protection Agency and the American Iron and Steel Institute for the joint support of this investigation.

1. INTRODUCTION

1.1 Setting of the problem

The metal industries in general, and the steel industries in particular, have a major impact on air pollution problems. Increasingly stringent environmental laws have generated new concerns and research needs about air quality. A summary of the different pollution sources from an integrated steelplant is presented in Fig. 1-1. As can be seen, emissions from steelplants can be divided onto particulates and gases. In the latter category, part of the byproducts emitted from coke ovens, sinterplants, pig iron casting operations, foundries, and rolling mills are hydrocarbons. Furthermore, hydrocarbon vaporization also occurs when remelting oily scrap or turnings, and during oil quenching operations.

Many processes have been developed to remove pollutants from off-gases, but little work has been done for lowering hydrocarbon concentrations down to, say, less than 0.5 g/cm^3, mainly because hydrocarbon removal has been thought of in terms of valuable byproduct recovery, and further recovery was not profitable. However, further removal could be very desirable for at least three reasons:

- Hydrocarbons vapors emitted from steelplants may contain aromatics which may be carcinogenic or cause neurological disturbances among steelplant workers (2).

- Hydrocarbon laden gases may cause plume opacity problems in workshops due to fine droplet condensation as the gases cool. At present, the existence of unsightly plume has been the main reason to examine the possibilities of removing hydrocarbon from effluent gases.

- Hydrocarbons have been found to poison the catalysts used in Japan to remove nitrogen oxides from steelplant emissions.

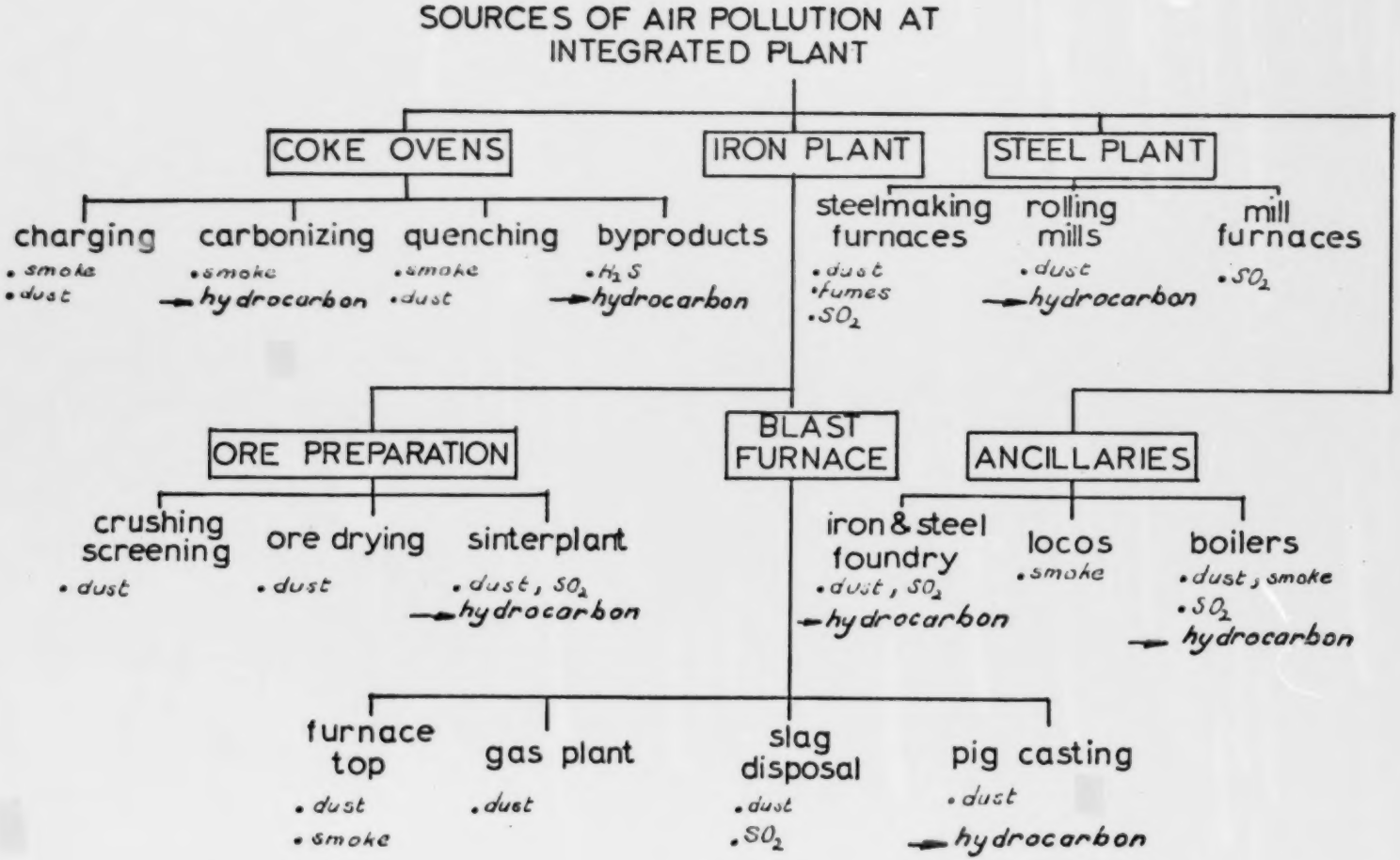

Figure 1.1 (from 1). Sources of air pollution at integrated plant.

1.2 Brief review of existing technologies

Generally, pollution control involves of a two-stage process, the first stage being devoted to particulate recovery, and the second stage to chemical recovery.

Particulate recovery systems can be a battery of cyclones, wet scrubbers, electrostatic precipitators, and/or bag houses; the devices are arranged in order of increasing efficiency for removal of the smallest particles [down to about 1 micron (3)].

The main chemical pollutants are nitrogen and sulfur oxides, and organic vapors. Technologies are available to remove such pollutants, but after the cleaning operations, the gases still contain the following residual loads in kg/ton of steel produced (3):

	SO_2	NO_x	hydrocarbons
sinterplant	1-12	0.3-0.8	0.02-0.2
coke ovens	0.2-5.0	0.2-2.5	0.2-2.0

These data have been obtained for point source emissions, that is to say emissions which leave the plant through well defined routes and are discharged outside. There might also be fugitive emissions of pollutants, for instance through door leaks, during handling of the scrap or the hot metal which are discharged inside the plant and almost impossible to quantify.

1.3 Solution under investigation

The proposed solution consists of using a fluidized bed of activated charcoal to remove, by phycial adsorption, hydrocarbons which are present in such low concentrations. Because of the presence of moisture which

will always be found in the effluent air streams to be cleaned, physical adsorption seems to be among the best available processes when flare system, conventional and catalytic afterburners, and absorbers become unefficient. A fluidized bed type process has been preferred to packed bed adsorbers because the pressure drop across the bed is minimized.

The purposes of this investigation can be summarized as follows:

- collection of data showing the reliability of the proposed fluidized bed adsorber in the laboratory,

- determining the optimal conditions under which hydrocarbons are adsorbed in preference to moisture, and

- deriving a mathematical model of the system which could be used for scale up calculation purpose.

2. LITERATURE SURVEY

Physical adsorption in fluidized beds is a very complex problem which has been extensively studied during the past decades. The first section of this survey will give a review of the different possible adsorption mechanisms which could be applied to the investigated system. The second section will present the necessary principles of fluidization as well as different proposed models of fluidized beds. The third section will discuss the choice of the adsorbent. In the fourth section, the nature of the hydrocarbons that are to be handled by the investigated process will be discussed, and the last section will review the applications of such systems on an industrial scale.

2.1 Physical adsorption

2.1.1. Definitions

When a gas is brought into contact with a solid, it has the tendency to collect on the surface. This phenomenon is known as adsorption. When the solid is a highly porous material, such as activated charcoal, activated alumina or silica gel, its internal surface area can be extremely high [more than 1000 m^2/g (4)]. The gas is able to penetrate inside the pores or micropores of the solid and thus is allowed to adsorb on the whole surface area. Such materials can collect an important amount of gas by physical adsorption. Physical adsorption is caused by van der Waals attractive forces and is similar in character to condensation of vapour molecules into a liquid of same composition (14). Physical adsorption is usually exothermic, the heat of adsorption being typically a few kcal/mole.

Physical adsorption requires no activation energy and therefore can occur nearly as fast as molecules strike the solid surface, but the overall rate of adsorption is also influenced by the diffusion into the gas film surrounding the solid surface as well as the diffusion of the adsorbate inside the pores of the solid.

The amount of adsorbed gas is usually related to p/p_o where p is the partial pressure of the vapour in the system and p_o is the vapour pressure that would exist above pure liquid at the same temperature. It has been found (14) that when p/p_o is less than 0.01, the amount of adsorbed species is negligible except with solids possessing fine pores; at values of about 0.1 to 0.3, the amount adsorbed corresponds to a monolayer coverage while a multilayer coverage is usually developed at values of p/p_o greater than 0.3, until essentially a bulk liquid is reached at $p/p_o = 1$.

On smooth surfaces, the van der Waals' adsorption is restricted to a layer of a few molecules thickness, while in a porous solid, capillarity condensation occurs in the pores (4).

2.1.2 Models of physical adsorption

As early as 1918, Langmuir (16) developed a model for the chemical adsorption mechanism, which was later extended to suppress multilayer physical adsorption by Brunauer, Emmet, and Teller (BET model) (17) in 1938. Langmuir's hypotheses, quoted by (12) are as follows:

1. Adsorption can take place only on certain sites and only one species can be adsorbed on a given site.

2. A monolayer coverage is assumed.

3. The adsorbed molecules cannot move from one site to another.
4. The surface energy distribution is uniform.
5. The adsorption on an empty site is not affected by the presence of adsorbed molecules on neighbouring sites.

From these assumptions, Langmuir derived that the adsorption rate was to be proportional to the number of unoccupied sites and to the partial pressure of the adsorbate:

$$\text{rate of adsorption} = k_1 \, p \, (1 - \theta) \tag{2.1}$$

and that the rate of desorption was to be proportional to the number of occupied sites:

$$\text{rate of desorption} = k_2 \, \theta \tag{2.2}$$

At equilibrium, the rate of adsorption must be equal to the rate of desorption and the covered fraction at equilibrium is:

$$\theta_{eq} = \frac{(k_1/k_2) \, p}{1 + (k_1/k_2)p} \tag{2.3}$$

where:

k_1 is the "foreward" rate constant

k_2 is the "reverse" rate constant

θ is the covered fraction

p is the partial pressure of the adsorbing gas

The BET analysis of adsorption is an extension of Langmuir's where the second basic assumption is relaxed. A multilayer coverage is assumed; it is also assumed that from layer 2 on, the heat of adsorption is the same for all layers and equal to the heat of liquefaction. The

BET model now leads to:

$$\frac{V}{V_m} = \quad = \frac{cx}{(1-x)(1-x+cx)} \tag{2.4}$$

where

$$x = m \frac{p}{n} \exp \frac{E_L}{RT}$$

with m, n = proportionality constants

E_L = heat of liquefaction

p = partial pressure of adsorbate

and $c = m' \exp \left(\frac{E_f - E_L}{RT}\right)$

with m' = proportionality constant

E_f = heat of adsorption on the 1st layer

V_m = volume of gas adsorbed when the first layer is completely filled.

V must tend towards infinity when $p = p_o$ (infinite number of layers) which implies $c = p/p_o$. It can also be seen that, at low pressures, Eqn. (2.4) reduces to Eqn. (2.3). Smith and Brunet (34) found that the BET model fits adsorption of propane and propylene on activated charcoal.

Two other models have also been derived: the Freundlich isotherm and the Temkin isotherm (10). The Freundlich isotherm, originally empirical, can also be derived theoretically by a statistical approach, in which the Langmuir isotherm of adsorptionis applied to a distribution of energies among the sites such that the heat of adsorption decreases logarithmically with coverage; the obtained relationship is:

$$\theta = c\, p^{1/n} \tag{2.5}$$

where c and n are constantswhich decrease as temperature increases.

In deriving the Temkin isotherm, a linearly rather than logarithmically decreasing heat of adsorption is assumed. Then, the relationship becomes:

$$\theta = \frac{RT}{q_o \alpha} \ln B \times p \qquad (2.6)$$

where

q_o = differential heat of adsorption at zero coverage

α, B are constants

2.1.3 Adsorption of multi-component mixtures

Gonzales and Holland (18, 19) developed a method for the determination of the adsorption equilibria of hydrocarbon mixtures in packed beds of activated charcoal. Their model was derived from the BET model but restricted to a 2-layer coverage; they showed that the amount of adsorption in all layers after the first one is small relative to the adsorption in the first layer.

The authors above have shown that continuous flow methods could be used to obtain the adsorption equilibrium data for multi-component systems.

Preferential adsorption is discussed by Fulker (49). The author stated that when mixtures of gases are adsorbed, the presence of each affects the equilibrium of the others. In general, a gas of high molecular weight, high critical temperature, and low volatility is adsorbed in preference to a gas of low molecular weight, low critical temperature, and low volatility. A preferentially adsorbed gas will displace other gases which have already been adsorbed.

2.1.4 Influence of temperature on the adsorption reaction

Satterfield (14) stated that the amount of gas physically adsorbed decreases monotonically with temperature, as readily shown in the Tenkin model; this agrees with the fact that desorption is an activated process (10), thus it is enhanced by increasing temperature.

The "foreward" and "reverse" rate constants are assumed to obey an Arrhenius relationship (20), i.e. activation energies and adsorption heat are assumed to be constant. Under these assumptions, they can be expressed in the following form:

$$k_1 = k_{1_0} \exp(-E_1/RT) \tag{2.7}$$

$$k_2 = k_{2_0} \exp(-E_2/RT) \tag{2.8}$$

where

k_{1_0} and k_{2_0} are constants

E_1 is the adsorption heat

E_2 is the desorption heat

Recalling Eqn. (2.3) at equilibrium

$$\theta = \frac{(k_{1_0}/k_{2_0})\, p \exp -(E_1-E_2)/RT}{1 + (k_{1_0}/k_{2_0})\, p \exp -(E_1-E_2)/RT} \tag{2.9}$$

which shows that E_1-E_2 must be negative, since adsorption is an exothermic process.

$\Delta H = E_1-E_2$ has been tabulated for many gases and is expected to increase proportionally to molecular weight for an homologous series, as of the paraffins (48, 14); this can be seen in Fig. 2-1 [adapted from (49)].

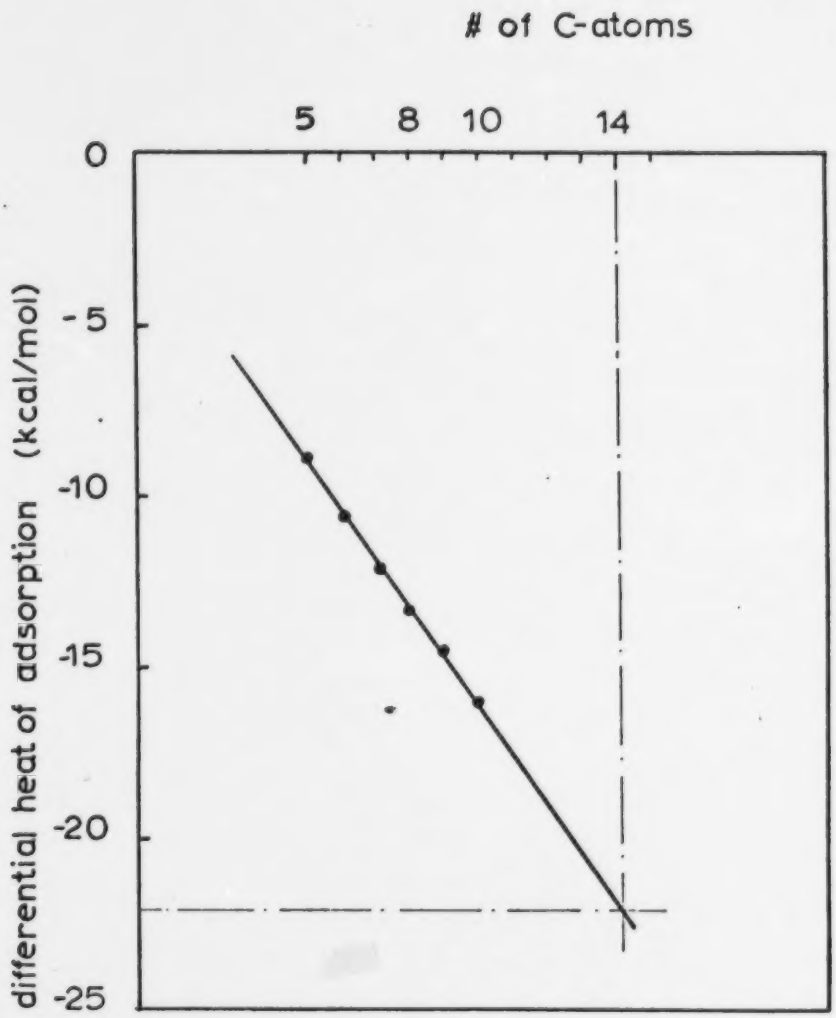

Figure 2-1. Heat of adsorption of n-alkanes.

2.2 Fluidization

2.2.1 Definitions

When a gas or liquid is forced to flow upwards through a bed of solid particles, a pressure drop is created across the bed. If this pressure drop becomes sufficient to support the weight of the particles, they become separated and free to move about; such bed is said to be incipiently fluidized (21, 22). Further increase in the gas velocity is generally accommodated by bed expansion and creation of bubbles. Despite the increase in gas flow, the pressure drop remains practically constant, until it drastically drops when the gas velocity reaches the elutriation velocity and solid particles are carried away from the bed. A diagram of pressure drop vs velocity is presented in Fig. 2-2 [from Shirai, quoted by (21)]. The maximum in this curve corresponds to the minimum fluidization velocity, under these conditions the particles are just supported by the gas; the following decrease in pressure drop is due to a rearrangement of the particles which leads to the smallest resistance arrangement.

Equations have been derived to quantify the pressure drop across the bed [Ergun (50)], the minimum fluidization velocity, and the terminal velocity (10, 21, 23).

2.2.2 Minimum fluidization velocity and terminal velocity

At minimum fluidization velocity, buoyancy forces are just equal to the weight of the bed, which can be written

$$A\Delta p = AL_{mf} (1-\epsilon_{mf}) g(\rho_s-\rho_g) \qquad (2.10)$$

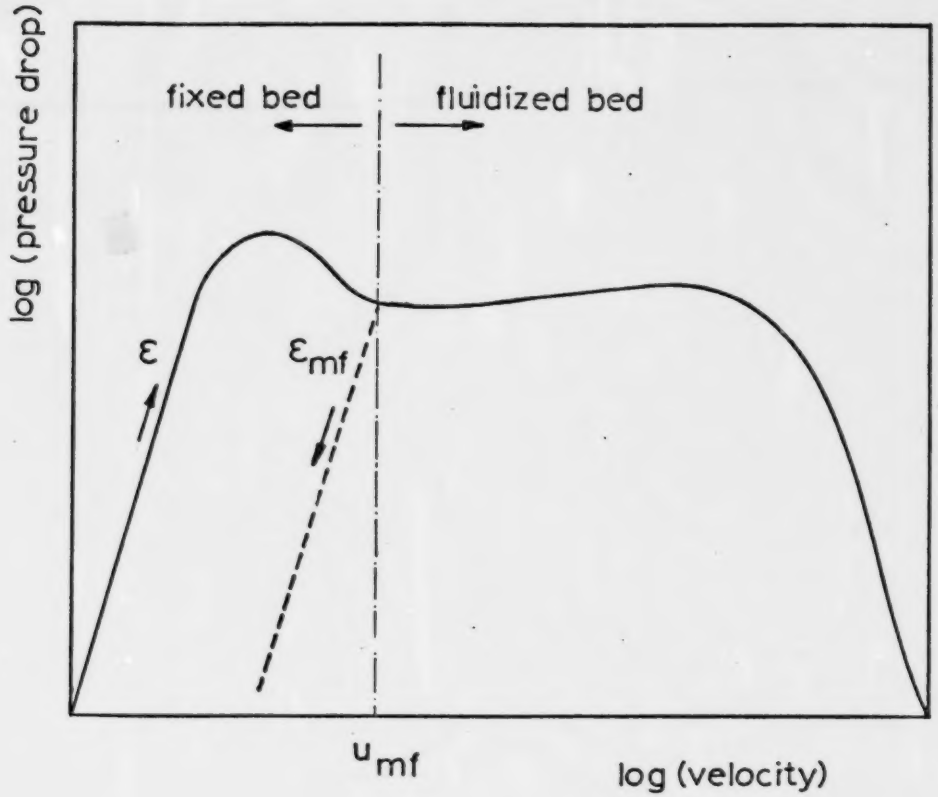

Figure 2-2. Pressure drop-velocity relationship.

substituting Ergun's equation for $\Delta p/L_{mp}$, a quadratic equation is obtained which is the sum of a viscous term and a kinematic energy term. In general depending on the particle Reynolds number, either one or the other may be neglected, to yield:

$$Re_p < 20 \qquad u_{mf} = \frac{(\phi_s d_p)^2}{150} g \frac{(\rho_s - \rho_g)}{\mu} \frac{\varepsilon_{mf}^3}{1-\varepsilon_{mf}} \tag{2.11}$$

$$Re_p > 1000 \qquad u_{mf} = \frac{\phi_s d_p}{1.75} g \frac{\rho_s - \rho_g}{\rho_g} \varepsilon_{mf}^3 \tag{2.12}$$

where

ρ_s and ρ_g are the solid and gas densities, respectively

ϕ_s is the shape factor

d_p is the particle diameter

ε_{mf} is the void fraction at minimum fluidization velocity.

The expression can be further simplified using the approximation proposed by Wen and Yu (5):

$$Re_p < 20 \qquad u_{mf} = \frac{d_p^2 \, g \, (\rho_s - \rho_g)}{1650\mu} \tag{2.13}$$

$$Re_p > 1000 \qquad u_{mf}^2 = \frac{d_p \, g \, (\rho_s - \rho_g)}{24.5 \, \rho_g} \tag{2.14}$$

The minimum fluidization velocity is computed using the value of the particle mean diameter.

Terminal falling velocity:

The terminal falling velocity is the velocity of a single falling-particle when gravity forces are just equal to the drag forces. In a fluidized bed, this corresponds to the minimum velocity above which the

particles will be carried away.

The gravity forces can be expressed by:

$$F_g = \frac{\pi}{6} d_p^3 (\rho_s - \rho_g) g \qquad (2.15)$$

Here again, the value of the drag forces depends on the particle Reynolds number (4):

$$10^{-3} < Re_p < 2 \qquad F_d = 3\pi d_p \mu u_t \qquad (2.16)$$

$$2 < Re_p < 500 \qquad F_d = \frac{2.31\pi d_p^2 \rho_g u_t}{g(Re_p)^{0.6}} \qquad (2.17)$$

$$500 < Re_p < 2x10^5 \qquad F_d = \frac{0.055\pi d_p^2 \rho_g u_t}{g} \qquad (2.18)$$

The first expression corresponds to Newtonian behaviour, the third to Stokes' behaviour, and the second one to a so-called "intermediate region".

The equations giving the terminal velocity are readily obtained (21):

$$Re_p < 0.4 \qquad u_t = d_p^2 \, g(\rho_s - \rho_g) \qquad (2.19)$$

$$0.4 < Re_p < 500 \qquad u_t = \left[\frac{0.0178 \, g^2 (\rho_s - \rho_g)^{2\ 1/3}}{\rho_g \mu}\right] \times d_p \qquad (2.20)$$

$$500 < Re_p < 2x10^5 \qquad u_t = \left[\frac{3.1 \, d_p g(\rho_s - \rho_g)\ 1/2}{\rho_g}\right] \qquad (2.21)$$

The terminal velocity is always computed for the smallest particles present in the fluidized bed: in some cases, when the particle size distribution is important, the minimum fluidization velocity of the bed can exceed the elutriation velocity of the fines.

2.2.3 Characterization of the particles

The shape and size of the particles have a great influence on the fluidization of the bed. Methods of characterization of the particles call for knowledge of the particle diameter, average particle diameter, shape factor or sphericity, specific surface area, and void fraction in packed beds. These characteristic values can be determined by scanning electron microscopy, as described by Byers et al. (45).

The equivalent particle diameter as defined by Kunii and Levenspiel (21) is:

$$d_p = \begin{matrix}\text{(diameter of sphere}\\ \text{(having the volume}\\ \text{(of the particle}\end{matrix} \qquad (2.22)$$

In general, this diameter is not directly accessible to measurement and must be approximated. For non-spherical particles a screen analysis generally overestimates d_p. This d_p value is used when computing the terminal velocity.

The average diameter of the particles can be defined in three different ways:

- arithmetic mean diameter: $$d_p = \frac{\sum_i b_i d_{pi}}{b_i} \qquad (2.23)$$

- volume mean surface diam.: $$d_p = \frac{\Sigma b_i d_{pi}^3}{\Sigma b_i d_{pi}^2} \qquad (2.24)$$

- specific area mean diam.: $$d_p = \frac{1}{\Sigma b_i / d_{pi}} \qquad (2.25)$$

where the b_i's are weighting factors which are related to the mesh size distribution.

The mean diameter value is used when computing the minimum fluidization velocity. When the mesh size distribution is small enough, the first definition is used (Eqn. 2.23) assuming only two sizes, the upper and lower mesh sizes.

The sphericity or shape factor is defined as follows:

$$\phi_s = \left(\frac{\text{surface of sphere}}{\text{surface of particle}}\right) \text{ of same diameter} \qquad (2.26)$$

$\phi_s = 1$ for spheres and is less than 1 for any other particle shape. Shirain, quoted by Kunii and Levenspiel (21) gives a value of $\phi_s = .691$ to .73 for pulverized coal and Szekely et al. (4) proposed a value of .65 for crushed coal.

The specific surface area of the particle is closely related to the two parameters, ϕ_s and d_p, by:

$$S_v = \frac{\text{surface of particle}}{\text{volume of bed}} = \frac{6(1-\varepsilon)}{\phi_s d_p} \qquad (2.27)$$

This is the value used for computing the overall mass transfer coefficient and should not be confused with the specific surface area of the particles which includes the internal surface of the pores. These two surfaces differ from each other by a factor of about 1000.

The void fraction is defined according to (4) as:

$$\varepsilon = \frac{\text{total volume of the bed-volume of solid particles}}{\text{total volume of the bed}}$$

The value of the minimum void fraction in a packed bed varies with the sphericity and the size of the particles but has a typical value of .45 for particles of sphericity ranges between .9 and .6, according to

Brown et al. quoted by (21).

Elutriation is directly related to the particle size distribution, since the broader the size distribution, the more fines and the lower the elutriation velocity. For experimental simplicity, the size distribution of fluidized particles has been chosen to be very narrow but elutriation cannot be completely neglected, since attrition, due to mechanical abrasion always happens in a fluidized bed. Merrick and Highley (23) and Lewis et al. (46) developed relations to describe elutriation rates. They concluded their analysis by stating that the elutriation material typically is comprised of about 65% fines originally in the bed, about 30% fines produced by abrasion and up to 8% produced by size reduction of coarser material to the assumed critical size for elutriation. The total rate of production of fines was found to be proportional to the difference $u-u_{mf}$ where u is the fludization velocity.

Other investigators, Gwyn, Blinichev et al., Zenz, [all quoted by Wen and Dutta (24)] propose other relations which seem to need further confirmation.

2.2.4 Flow patterns

2.2.4.1 Solid flow patterns

A vast amount of literature has been published on this subject and it appears that a high degree of solid mixing exists in fluidized beds.

Solid size, bed diameter, gas distributers and fluidization velocity seem to be the most influential parameters in the quality of mixing. Evidence of this is found in the radioactive tracer experiments carried out by May, Leva and Grummer, quoted by Schulte (11). The authors state that mixing is described by Fick's law:

$$\frac{\partial C}{\partial t} = D_s \frac{\partial^2 C}{\partial z^2} \qquad (2.28)$$

where C is the tracer concentration and D_s the solid phase diffusivity. D_s has been found to increase as the bed diameter increases (May).

Data from Bart, quoted by Schulte, could fit the relationship:

$$C = C_o \exp(-s/E_s)z \qquad (2.29)$$

where E_s/s is the mixing length in the solid phase

E_s is the solid diffusion coefficient

Most of the authors agree that longitudinal mixing in a fluidized bed is very intense while radial mixing is less evident. However, in the rest of this study, solid back mixing (both radial and longitudinal) will be assumed--which is thought to be reasonable for the small beds to be used in this work.

2.2.4.2 Gas flow patterns

The gas flow patterns in fluidized systems are always difficult to define and are very likely to be greatly influenced by the presence of bubbles, shape and size of particles, and gas distributors.

Again, radioactive tracer techniques were used by Gilliland et al. [quoted by (11)] and appreciable mixing was found. The same investigators found that backmixing of gas near the bed walls and bypassing of the gas in the rising bubbles occurred. It was suggested that larger height of bed to bed diameter ratios result in a piston flow pattern while lower I/D ratios favor complete mixing.

Kunii and Levenspiel (21) derived a model in which backmixing of the gas was assumed, as well as a certain amount of bypassing of the

gas; Hatfield and Amundson (28) further approximated the fluidized bed as two parallel beds, with the major portion of the gas flow through the solid phase, in which backmixing is assumed, and with the rest of the gas merely in a bypass stream around the solid phase.

2.2.5 Bubbling in a fluidized bed

Grace has written a thorough review of these proposed models (29). In most of the models, the main assumption is the consideration of two or three distinct phases: a dense phase containing interstitial gas and virtually all of the solid and a bubble phase consisting of discrete void regions moving upward through the bed; this phase can be further broken up into a bubble phase and a cloud phase which consists of solid particles at the interface of the bubble and solid phases. Grace's conclusion is worth quoting:

> "Many of the models for predicting reaction rates in fludized bed reactors are based on the behaviour of isolated bubbles. At this time, there appears to be no reason for having greater confidence in bubbling model than in simpler two-phase models or for preferring a particular model.-. (but) bubble interactions have important consequences, especially with respect to gas-solids contacting."

Although Grace's article is 7 years old, no satisfactory overall bubbling theory has yet been presented even though a proposed model may have an excellent fit with a specific system (37, 41, 42, 43).

2.3 Activated Charcoal

Activated charcoal is a widly used adsorbent, because of its non-polar and highly porous structure which gives it a large adsorption capacity (31). It can be manufactured from a wide range of carbonaceous substances. After Lamb et al. [quoted by Fulker (49)], the raw material is a compound of amorphous carbon and hydrocarbons, not in itself active but becoming active when the hydrocarbons are removed by oxidation.

The activation of charcoal can be done either by steam or chemical reaction and the choice of the activation process and the raw material determine the physical properties and the adsorption capacity of the carbon. Nowadays, activated charcoal has two fields of application: recovery of impurities--vapors, odors, pollutants--and gas masks.

Activated charcoal has a strong selective power for the adsorption of organic vapors from gases (19, 32, 33, 34, 35) even in the presence of water vapor (49) and has great advantage over other solvent recovery systems--refrigeration, condensation, absorption--in its outstanding ability to recover solvents from low concentrations.

There exist many methods of regeneration, including:

- heating the adsorbent until the vapor pressure of the adsorbate exceeds atmospheric pressure,
- lowering the total pressure below the vapor pressure of the adsorbate,
- withdrawing the adsorbate by passing a stream of inert gas through the adsorbent keeping the partial pressure of the stripped gas below the equilibrium pressure of the adsorbate,

- withdrawing the adsorbate in steam (steam regeneration) and recovering in a condenser,
- displacing the adsorbate by a preferentially adsorbed gas.

Of the 5 proposed methods, steam regeneration seems to be most widely used (21, 32, 49).

2.4 Hydrocarbons

In this section, a quick review will be made of the nature of the hydrocarbons which are to be handled by the investigated process; such hydrocarbons are very likely to be present in the coke oven environment (see Fig. 1-1). The gases leaving the ovens contain light oil (36) characterized by a specific gravity of about 0.880. This oil is a mixture of all those condensable products of coal gas with boiling points less than 200°C, containing well over a hundred constituants, as can be seen in Fig. 2-3. The coke oven gases are purified by any of the following methods:

- refrigeration and compression, involving temperatures below -70°C and pressures up to 10 atm.
- adsorption by solid adsorbents involving the removal of light oil from the gas by passing it through a bed of activated charcoal and recovering the light oil from the carbon by heating with direct or indirect steam.
- absorption by solvents involving washing the coal gas with a petroleum wash oil, a coal tar fraction, or other absorbent, followed by steam distillation of the enriched absorbent to recover the light oil.

CONSTITUENT GROUP	FORERUNNINGS (2% of Light Oil)			CRUDE BENZENE (60% of Light Oil)			CRUDE TOLUENE (18% of Light Oil)		
AROMATICS	Traces of Benzene			Benzene	C_6H_6	80.1° C.	Toluene	$C_6H_5CH_3$	110.6° C.
PARAFFINS	n-Pentane	C_5H_{12}	36.1° C.	n-Hexane 2-Methylhexane n-Heptane	C_6H_{14} C_7H_{16}	68.8° C. 90.3° C. 98.4° C.	n-Heptane n-Octane	C_7H_{16} C_8H_{18}	98.4° C. 125.6° C.
CYCLOPARAFFINS NAPHTHENES	Cyclopentane	C_5H_{10}	51.0° C.	Cyclohexane	C_6H_{12}	80.8° C.	Methylcyclohexane Cycloheptane	$C_7H_{13}CH_3$ C_7H_{14}	100.3° C. 120.3° C.
UNSATURATEDS (Olefins-Diolefins and Aromatic Hydrocarbons with Unsaturated Side Chains)	Butene-1 Pentene-1 Amylenes n-Hexylene Cyclopentadiene-1, 3 Butadiene-1, 3	C_4H_8 C_5H_{10} C_6H_{12} C_5H_6 C_4H_6	−6.5° C. 30.1° C. 20 to 41.0° C. 61.0° C. 42.0° C. −5.0° C.	Hexene-2 Hexadiene-1, 3 n-Heptylene Cycloheptene Unidentified Compounds	C_7H_{14}	99.0° C. 85.0° C.	Unidentified Compounds		
SULPHUR COMPOUNDS	Carbon Disulphide Hydrogen Sulphide Hydrogen Cyanide Carbonyl Sulphide Methyl Mercaptan Ethyl Mercaptan Dimethyl Sulphide	CS_2 H_2S HCN COS CH_3SH C_2H_5SH $(CH_3)_2S$	46.3° C. −59.6° C. 26.0° C. −50.2° C. 7.6° C. 34.7° C. 36.2° C.	Thiophene Diethyl Sulphide	C_4H_4S $(C_2H_5)_2S$	85.0° C. 91.6° C.	Methylthiophene	C_5H_6S	112 to 115.0° C.
NITROGEN & OXYGEN COMPOUNDS							Pyridine	C_5H_5N	115.3° C.

CONSTITUENT GROUP	CRUDE NO. 1 SOLVENT (8% of Light Oil)			CRUDE NO. 2 SOLVENT (6% of Light Oil)			CRUDE RESIDUE (6% of Light Oil)	
AROMATICS	o-Xylene m-Xylene p-Xylene Ethyl Benzene	$C_6H_4(CH_3)_2$ $C_6H_5C_2H_5$	141.0° C. 139.1° C. 138.4° C. 136.2 C.	n-Propyl Benzene Ethyl Toluenes Mesitylene Pseudocumene Hemimellitene Cymenes Durenes	C_9H_{12} $C_6H_3(CH_3)_3$ $C_{10}H_{14}$ $C_6H_2(CH_3)_4$	158.6° C. 161.2 to 161.9° C. 164.6° C. 169.2° C. 176.2° C. 175.5 to 177.3° C. 196.0 to 198.0° C.		
PARAFFINS	n-Octane n-Nonane	C_8H_{18} C_9H_{20}	125.6° C. 150.7° C.	n-Decane	$C_{10}H_{22}$	171.0° C.		
CYCLOPARAFFINS NAPHTHENES	Cyclooctane	C_8H_{16}	150.0° C.	Cyclononane	C_9H_{18}	172.0° C.		
UNSATURATEDS (Olefins-Diolefins and Aromatic Hydrocarbons with Unsaturated Side Chains)	Octylene Styrene Unidentified Compounds	C_8H_{16} C_8H_8	126.9° C. 146.0° C.	Coumarone Dicyclopentadiene Indene	C_8H_6O $C_{10}H_{12}$ C_9H_8	175.0° C. 170.0° C. 182.0° C.	Wash Oil Naphthalene Solvents Pitch Residue	275 to 360.° C. 218.° C. Above 200.° C.
SULPHUR COMPOUNDS	Thioxenes	C_6H_8S	137 to 146.0° C.	Trimethylthiophene Thiophenol Tetramethylthiophene		160 to 163.0° C. 169.5° C. 182 to 184.0° C.		
NITROGEN & OXYGEN COMPOUNDS	Picolines	C_6H_7N	131 to 143.0° C.	Cresols Dimethyl Pyridines Phenol	C_7H_8O C_7H_9N C_6H_6O	190 to 203.0° C. 143 to 161.0° C. 182.0° C.		

Figure 2-3. Fractions of coke-oven kight oil, and boiling points of some of their constituents. (Used with permission of U. S. Steel Corp.)

Reproduced from best available copy.

The percentage removed lies in the range of 90 to 95% so that the contamination level in the purified gas falls well within the concentration range investigated in this study.

2.5 Adsorption in fluidized beds; scale up

The adsorption in a fluidized bed has been well studied and a large amount of literature is available on this subject concerning a great variety of adsorbents and adsorbates: removal of sulfur compounds (38, 39, 44), drying of materials (40), adsorption of moisture (33), etc.

In comparison, little literature is available concerning the scale up of such adsorbers, although Ermenc (47) discussed their design in 1961 and Kunii and Levenspiel in 1969. Avery and Tracey (32) described the plant design of a multistaged fluidized adsorber for the recovery of carbon disulfide or other solvents from air or gas streams. In this design, adsorption and stripping of the charcoal takes place continuously in two separate vessels. The adsorber consists of a series (5 to 10) of stacked shallow beds, 2 to 3 in. deep and 40 ft. in diameter giving almost 100% tray efficiency (see Fig. 2-4), and was capable of handling 10,000 to 500,000 scfm.

This process has been successfully used for recovering acetone, ethanol, ethyl acetate, and carbon disulfide from air streams, with concentrations ranging from 500×10^{-9} g/cm^3 (CS_2 in Balakavo, USSR) to 65×10^{-6} g/cm^3 (ethanol in London, England). The selection of adsorption efficiency is a matter of economic balance between the value of increased solvent recovery and the cost of additional stripping steam. The optimum efficiency was found to be around 99% in 1968 and is very likely to be

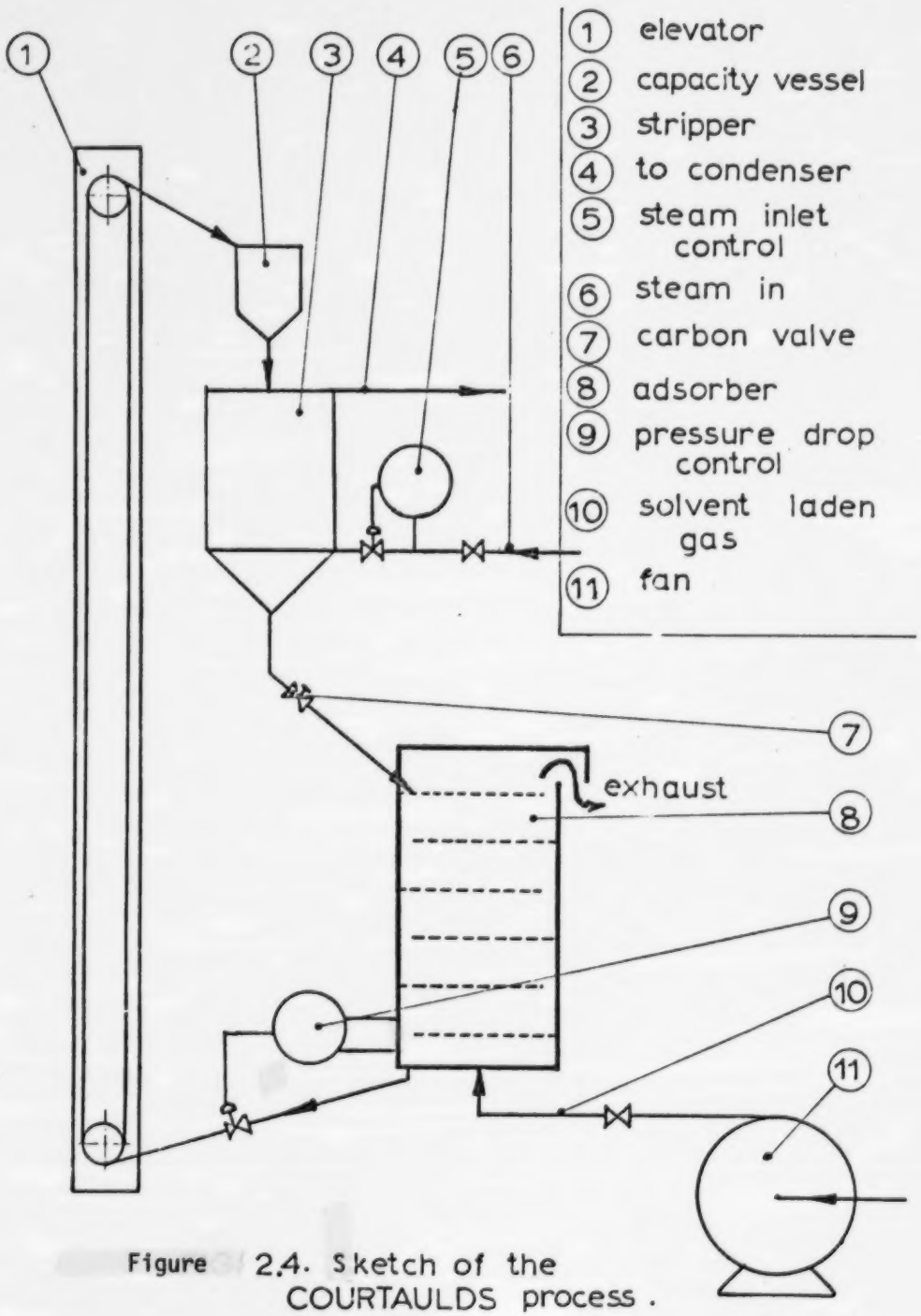

Figure 2.4. Sketch of the COURTAULDS process.

increased due to stricter environmental legislation.

2.6 Summary of the literature survey

In summary, it seems that physical adsorption in a fluidized bed of activated charcoal can provide a reliable means for removing hydrocarbon vapors from effluent air streams (21, 31, 32, 38, 39, 40, 44). It is expected that the adsorption mechanism will be well described by the B.E.T model since the involved partial pressures of hydrocarbon will be low indeed (4, 14, 34). By varying the temperature of the bed and of the inlet gas, it is hoped that the mechanisms of preferential adsorption will favor the removal of hydrocarbon rather than the removal of moisture (14, 43). Also, it is expected that a shallow fluidized bed will insure a good mixing of the solids (21) and allow for neglecting the formation of bubbles (29).

The experimental verification of these ideas will be the subject of this work.

3. APPARATUS AND EXPERIMENTAL METHOD

3.1 Apparatus and experimental method

3.1.1 Description of the apparatus

A sketch of the laboratory apparatus is given in Fig. 3-1. This apparatus allows the passing of a gas of known composition through a fluidized bed of activated charcoal and provides facilities for the analysis of the exit gas.

An air stream from a cylinder of compressed air [1] is passed through two filters containing silica gel [2] and activated charcoal [3] to remove all traces of water and hydrocarbon which could be present in this air stream. This purified stream is then split into two streams, both metered by a rotameter [5]. The lower stream passes through a saturator [6] containing the hydrocarbon under investigation. The upper air stream may or may not be passed through another saturator [7] containing water. Both streams are then joined to pass through the fluidized bed of activated charcoal [10]. Valves are arranged to allow the analysis of the inlet or the outlet gas in the analytical gas chromatograph [13]. Heaters [8, 9], regulated by the temperature controller [11], provide a means of selecting the temperature for a given run. Both the gas chromatograph and temperature controller outputs are recorded on a strip chart [12].

3.1.2 Analytical gas chromatograph

The gas was analyzed in an AGC-311 analytical gas chromatograph manufactured by CARLE INSTRUMENTS, INC. (Fullerton, Ca). This AGC can provide both thermal conductivity detection (TCD) and flame ionization detection (FID). Practically, only FID was used, being much more sensitive to low hydrocarbon concentrations. Fig. 3-2 shows a sketch of

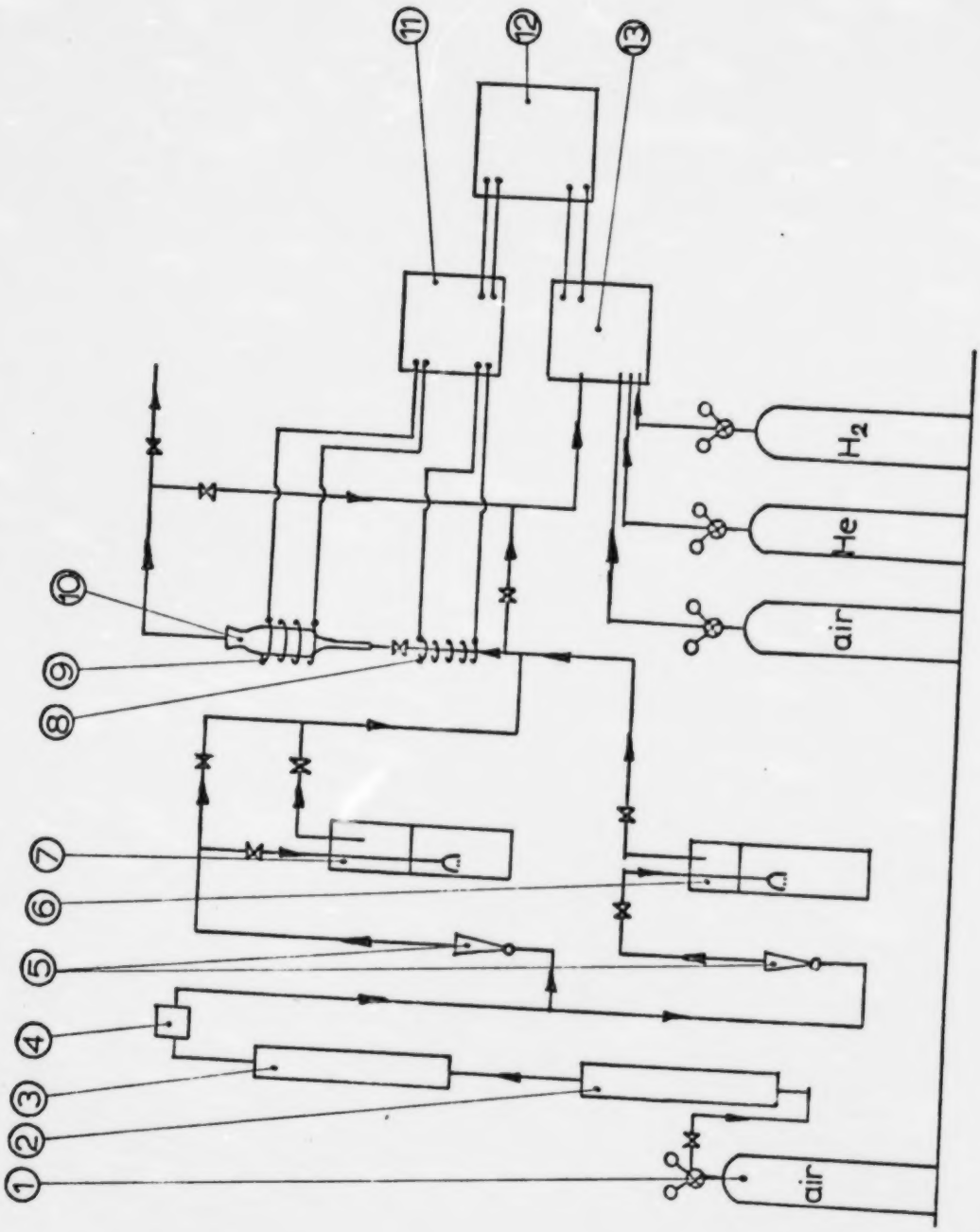

Figure 3-1. Sketch of the apparatus.

① cylinder of compressed air

② silica bed

③ charcoal bed

④ filter

⑤ rotamers

⑥ hydrocarbon saturator

⑦ water saturator

⑧ inlet heater

⑨ fluidized bed heater

⑩ fluidized bed

⑪ temperature controller

⑫ recorder

⑬ gas chromatograph

Figure 3-1. Sketch of the apparatus.

the AGC. The capabilities of this apparatus are:

- column temperature control ranging from 0°C to 399°C, by 1°C increments, with an accuracy of 10^{-3} °C.
- using a single jet quartz burner, fed from both columns, the apparatus has a large flame which minimizes the effects of background noise.
- the apparatus is sensitive in the range of 1 picogram to 1 milligram.
- the sampling is performed by a microvalve (CARLE No.5518) which allows for injecting exactly the same amount of gas (5 cm^3) for each run which insures the repeatability of the measurement. A sketch of this valve is given in Fig. 3-3.

3.1.3 Description of an experiment

After the charcoal has been dried overnight at 80°C, it is weighed on an analytical balance (typical sample weight is 0.6 gram, this gives a height when fluidized of about 0.3-0.4 cm). The apparatus is then purged for about an hour by blowing pure air through the tubings and the bed; its cleanliness is checked by analyzing the exit gas.

The temperature of the bed is then set and the fluidized bed of charcoal is installed. Its weight variations are recorded until stabilization to insure the equilibrium of the temperature and of the charcoal-pure air system.

The lower air stream is then allowed to pass through the hydrocarbon saturator, and if desired, the upper air stream is passed through the water saturator; the flow rates are set at desired levels to meet the

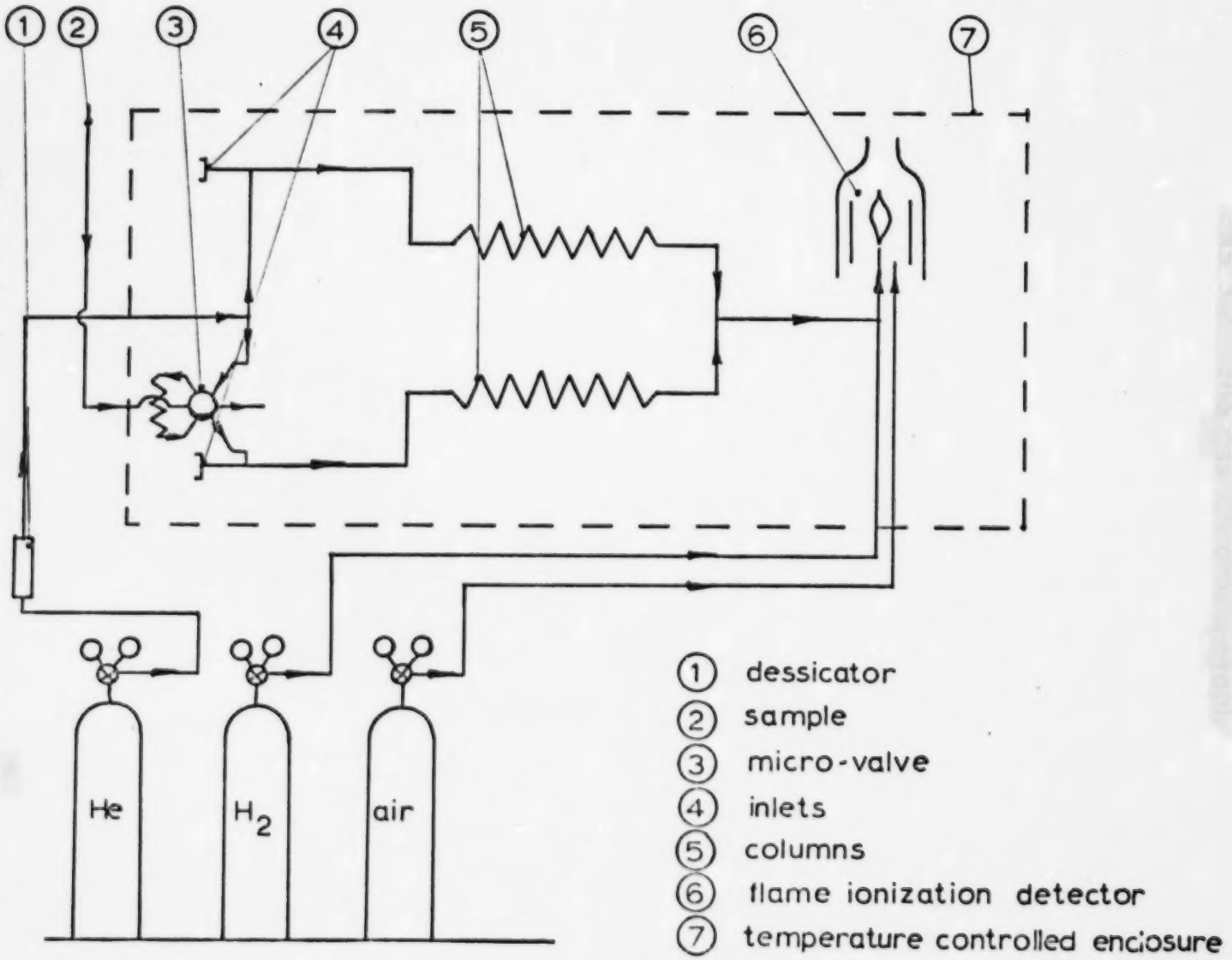

Figure 3-2. Sketch of the analytical gas chromatograph.

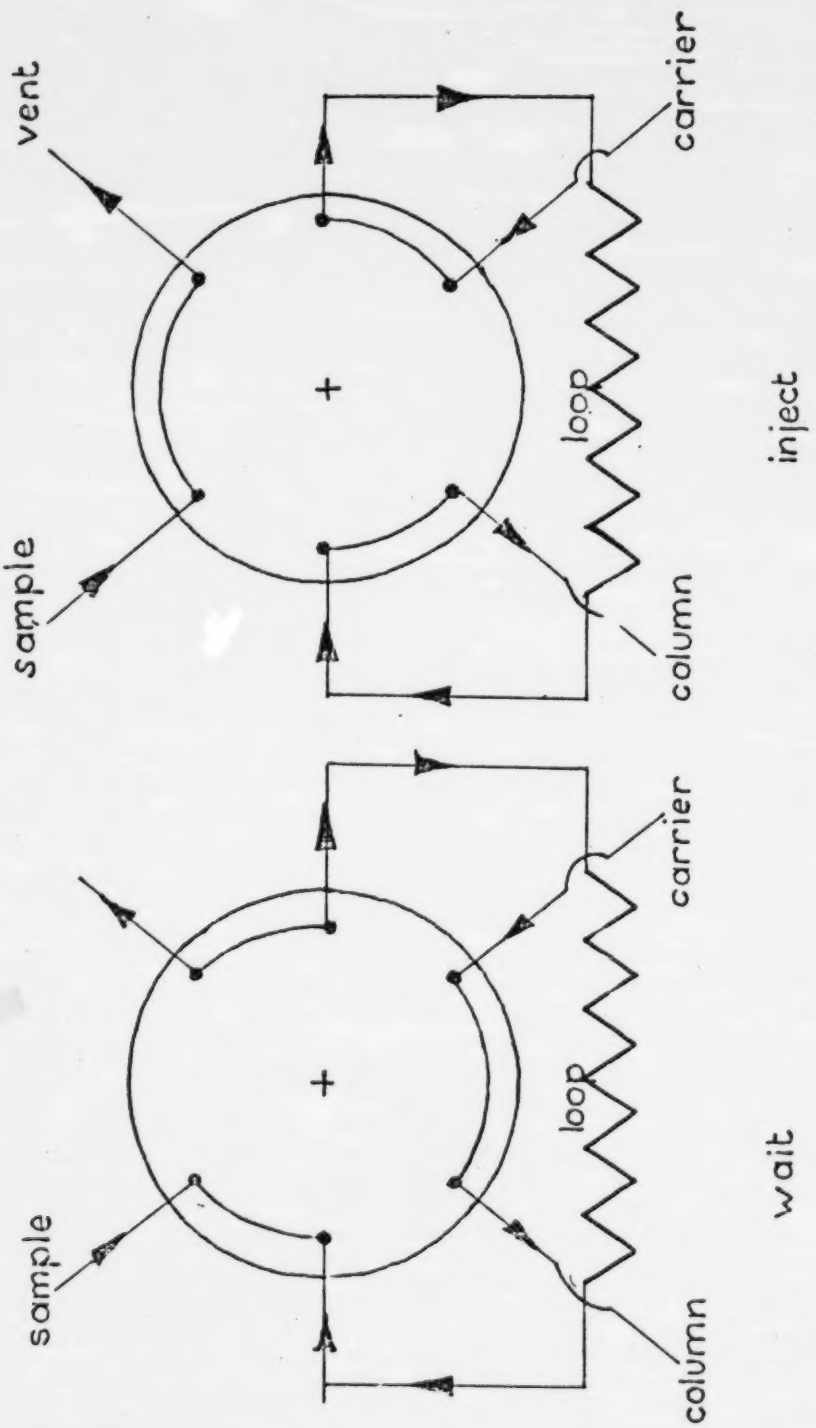

Figure 3-3. Sketch of the micro-valve.

chosen hydrocarbon concentration and the adsorption reaction takes place.

The exit air stream is analyzed every 30 minutes until the charcoal reaches saturation. Then the inlet air stream is analyzed. The typical duration of an experiment is 5 to 6 hours.

3.1.4 Analysis of an experiment

The composition of the air stream is determined by gas chromatography. Briefly, in the AGC, the air stream is passed through a temperature controlled column where the components of the stream are adsorbed, then desorbed, at different retention times according to different physical properties such as molecular weight, polarity, shape, etc.

After desorption, a particular component is burnt in the hydrogen flame of the FID and the change of ionization of the burnt gases causes the deflection of the pen of the recorder. A component is thus characterized by a peak on the recorder chart, the area of which is proportional to the mass of the component reacted. By knowing the sample volume, the concentration of the given species can be determined.

Calibration of the AGC is required for each possible component. This is accomplished by injecting (with a syringe) known amounts of the component and measuring the corresponding peak area. There are many methods of determining the peak area; since the peak shape could be approximated by an isoceles triangle, the method used consisted of cutting out the peaks and weighing the paper. Assuming the chart paper density to be the same throughout the peaks, and having weighed a square inch of it, it is then easy to calculate the peak area from its weight.

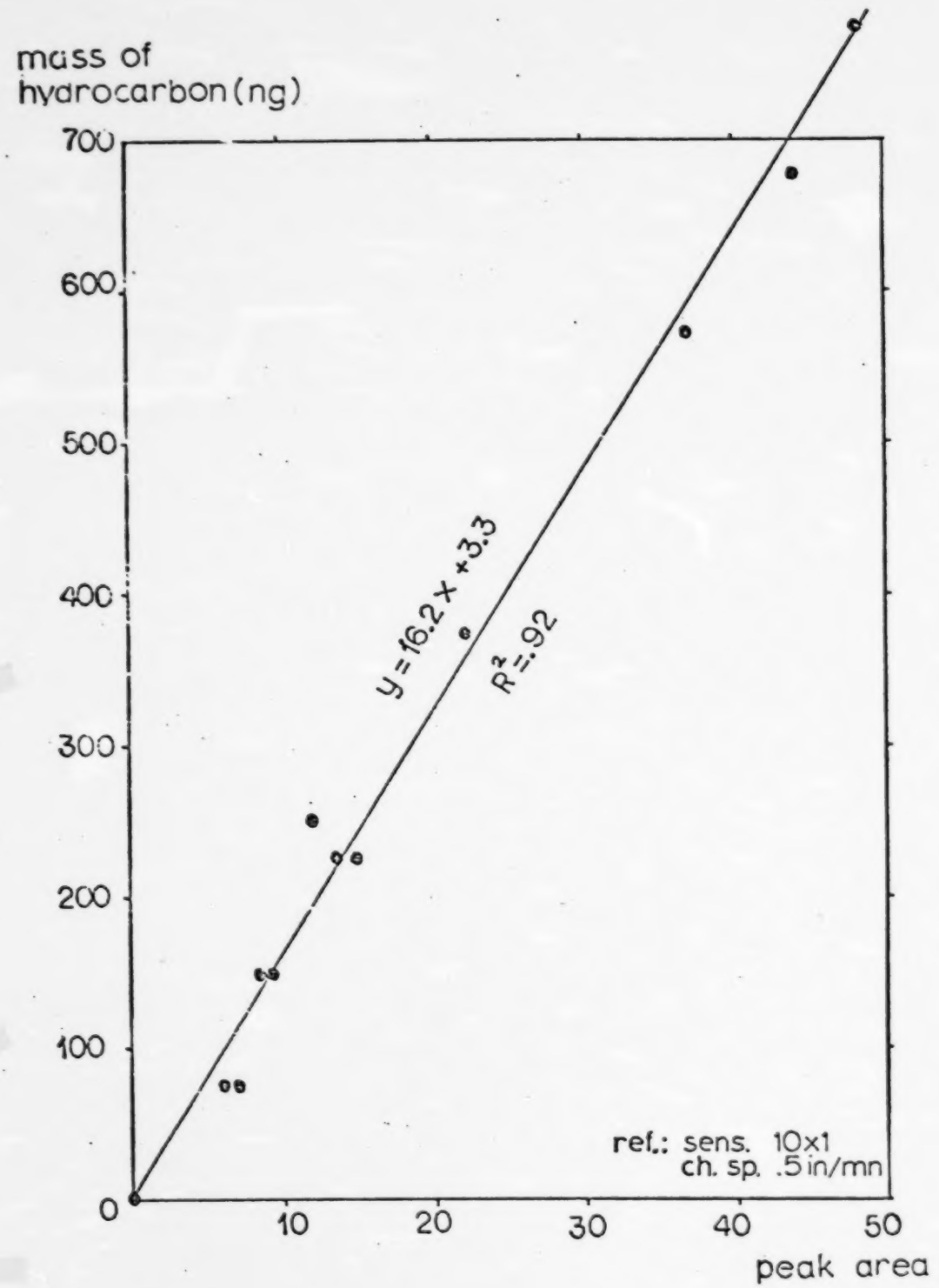

Figure 3.4. Calibration of the gas chromatograph.

The calibration of the gas chromatograph with respect to n-tetradecane is shown in Fig. 3-4. The relationship between amount of hydrocarbon and peak area is linear as expected. The equation of the line was determined by the least squares method, and exhibits a reasonable correlation coefficient: $R^2 = 0.92$.

From the recorder chart, the variation of the hydrocarbon present in the gas versus time can be determined. It is then possible to calculate the mass of hydrocarbon adsorbed on the sample, using:

$$m_{HC,ads} = \int_0^t (C_f - C_e)\ \dot{v}\ dt$$

where

t is the time

C_f is the gas feed concentration

C_e is the hydrocarbon exit concentration

$\dot{v}$ is the gas flow rate

It is then possible to determine the amount of moisture adsorbed by weighing the sample, since

$$\Delta m = m_{HC,ads} + m_{H_2O,ads}$$

A typical gas analysis is presented in Fig. 3-5. As can be seen, a given component is characterized by its retention time:

1 min for the air

2 min for the moisture

12 min for the n-tetradecane

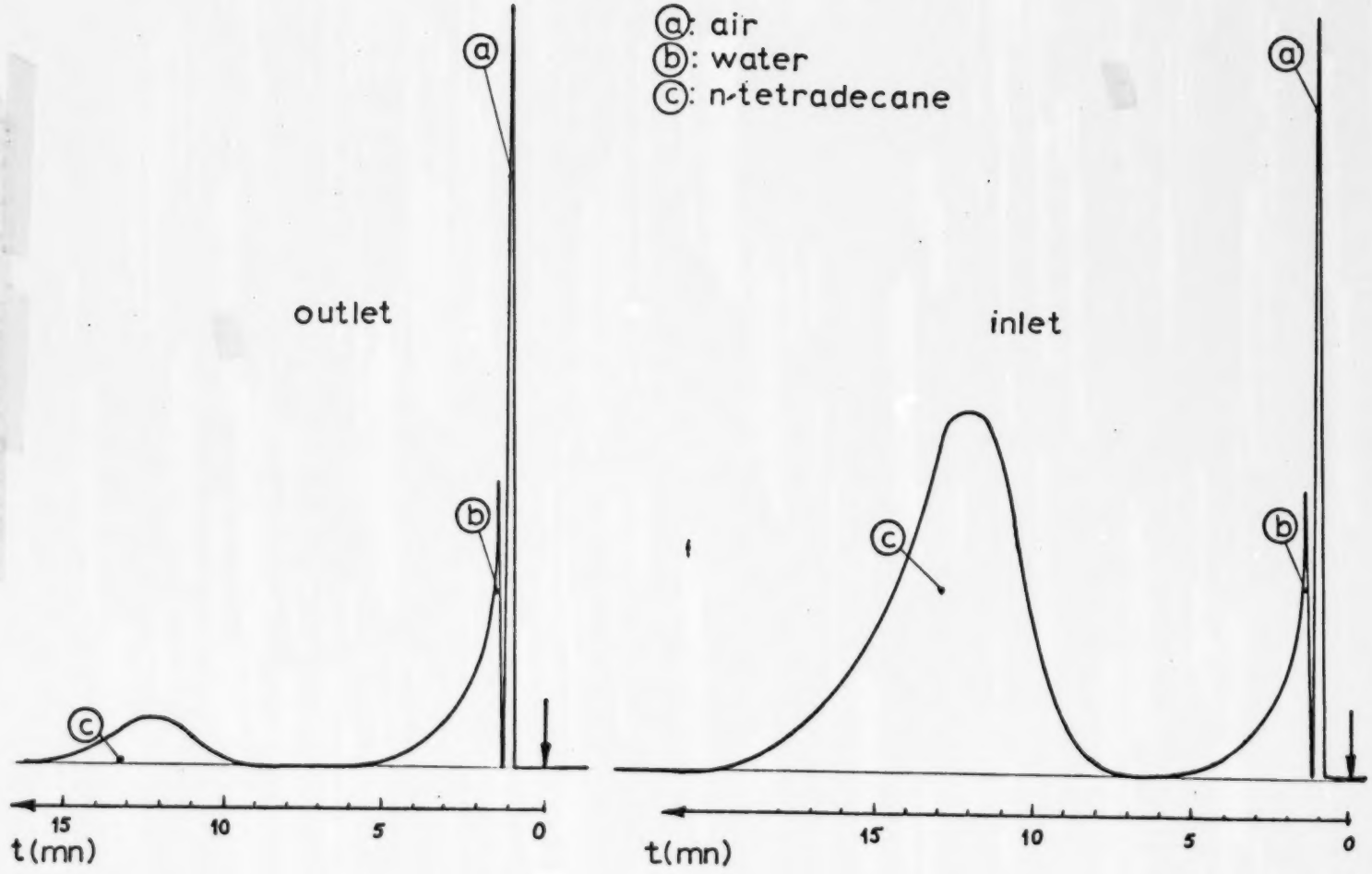

Figure 3-5. Chromatogram.

This chromatogram also shows the reliability of the method: the water peak (b) has the same area in the inlet and outlet gas, while the hydrocarbon peak is much smaller in the outlet gas than in the inlet gas.

3.2 Parameters influencing the experiments

The most important parameters have been found to be:

- The choice of the adsorbent
- The choice of the adsorbate
- The temperature of the bed
- The fluidizing velocity, height of the bed, particle diameter, hydrocarbon feed concentration

3.2.1 Choice of the adsorbent

The most commonly used adsorbents are: activated charcoal, activated alumina, silica gel, and molecular sieves. For these experiments, an adsorbent which could selectively adsorb hydrocarbon from a hydrocarbon and moisture laden gas had to be selected. Preliminary experiments were carried out using activated charcoal and activated alumina, the results were that the activated charcoal was found to be much more efficient than the alumina.

Typical experiments involving activated alumina are presented in Figs.3-6 and 3.7, the results of which can be summarized in Table 3-1.

Experiment A5 differs from experiments A3 and A4 in that a much deeper bed of alumina was used (10 and 3 mm respectively when fluidized). At room temperature, alumina tends to adsorb moisture preferentially, and at higher temperature, the hydrocarbon removal efficiency is not very satisfactory (56% compared to 90% for charcoal). Furthermore, in

TABLE 3-1. SUMMARY OF RESULTS INVOLVING ACTIVATED ALUMINA, THE AIR STREAM BEING SATURATED IN MOISTURE AT ROOM TEMPERATURE.

run	temp. (°C)	inlet conc, g/cm^3	durat. of run mn	hydroc. removed %	moisture adsorbed mg	hydroc. adsorbed gmol/g
A3	25	0.18×10^{-7}	240	57	77.2	8.7×10^{-5}
A4	80	0.57×10^{-7}	300	56	2.0	35.5×10^{-5}
A5	65	0.36×10^{-7}	180	28	195	$.5 \times 10^{-5}$

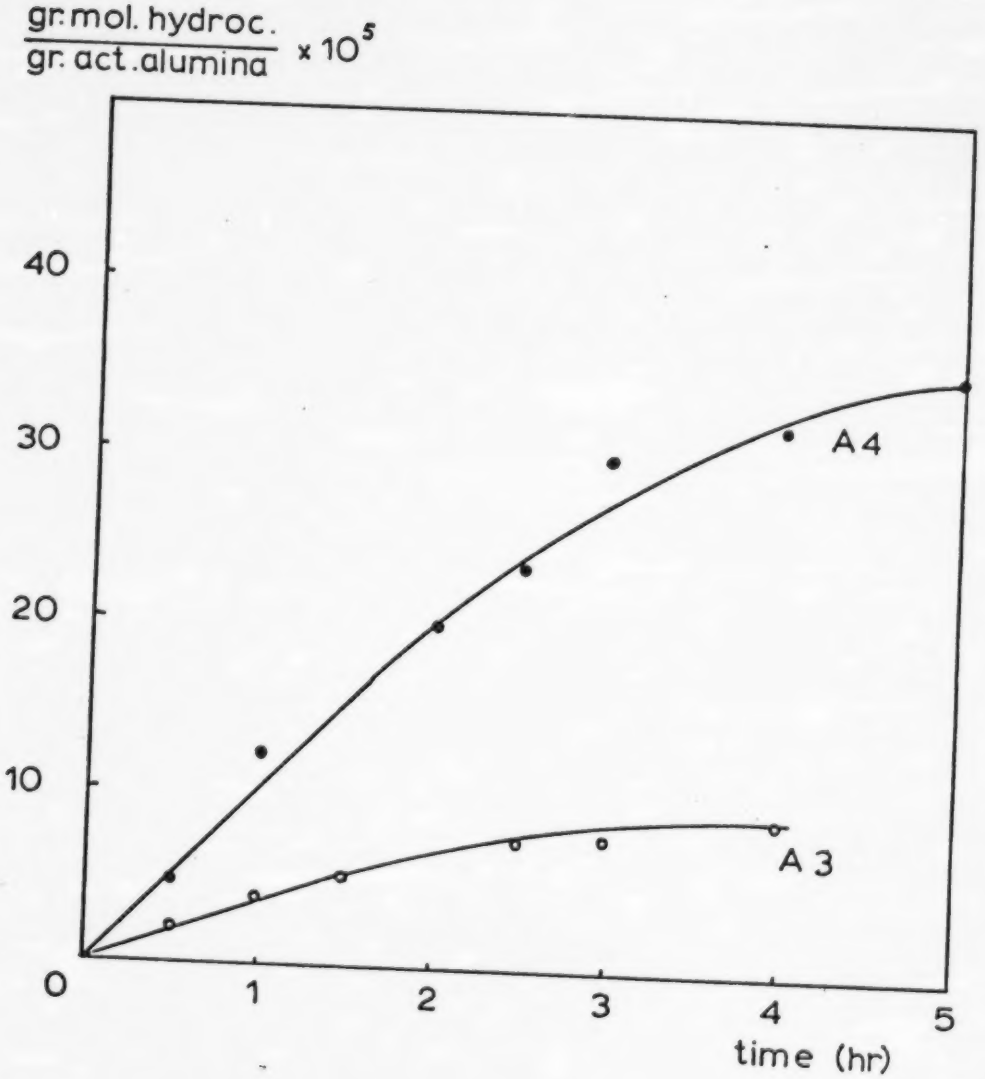

Figure 3-6. Adsorption of n-tetradecane on activated alumina.

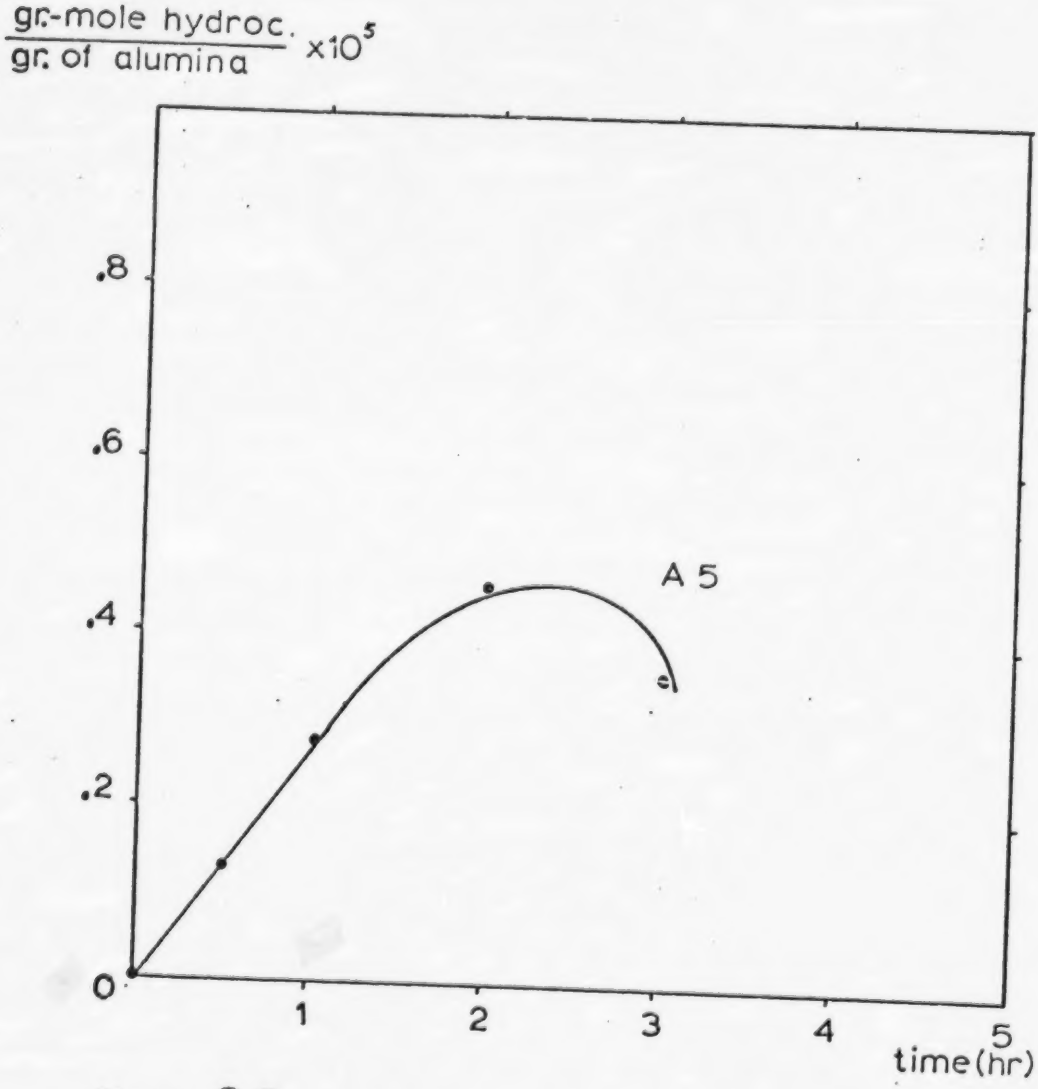

Figure 3.7. Adsorption of hydrocarbon on a deep bed of activated alumina.

deeper beds, the moisture tends to displace the hydrocarbon as time progresses.

However, it must be emphasized that activated alumina is a difficult material to work with because it adsorbs moisture very rapidly at room temperature, and one cannot be sure it is perfectly dry at the beginning of an experiment.

A confirmation of these findings can be found in the literature (49), where R.D. Fulker stated that silica gel, activated alumina, and molecular sieves will preferentially adsorb moisture from a gas containing both hydrocarbon and water vapours.

3.2.2 Choice of the adsorbate

The hydrocarbons which are to be handled by the investigated system will generally consist of a complicated mixture of different organic vapors (see Sect. 2.2.4). Due to the difficulty of studying such mixtures, it was thought that investigating a single well defined component would be of considerable simplification but still be fairly representative of reality.

N-tetradecane was chosen because of its inertness with activated charcoal because it is a saturated paraffinic chain; its definition and properties are well known (54). It was also readily available.

3.2.3 Temperature of the bed

Preliminary experiments showed that at room temperature, a fluidized bed of activated charcoal can remove 90-95% of the hydrocarbon content of an inlet air stream; the same system cannot selectively remove hydrocarbon from a moisture laden gas stream.

When heated to higher temperature (up to 125°C), this system does not adsorb any more moisture, but still adsorbs hydrocarbons, although the ability to adsorb hydrocarbons, is somewhat reduced due to desorption being an activated process.

This proves that there must be an optimal temperature at which moisture is not adsorbed and hydrocarbon is still removed in satisfactory amounts.

Experiments have been carried out with several bed temperatures; a summary of these is presented in Table 3-2 and in Fig. 3-8. According to these results, the optimal operating temperature was found to be 80°C.

It may seem paradoxical although it is well known that adsorption capacity decreases with temperature, that an increase of the capacity was recorded between room temperature and 80°C. However, these results are inherently self consistent since the hydrocarbon and moisture are competing to be adsorbed on a given site. Both the moisutre and hydrocarbon capacities are lowered as temperature increases, but the latter decreases much slower than the former, thus more sites are available for the adsorption of the hydrocarbon. The amount of hydrocarbon removed in the presence of water vapor is actually greater at 80°C than at room temperature.

3.2.4 Fluidization velocity

The gas fluidization velocity has a great influence on the removal efficiency of the bed.

TABLE 3-2. ADSORPTION OF HYDROCARBON ON ACTIVATED CHARCOAL

run	temp (°C)	inlet conc, g/cm^3	durat. of run mn	hydroc. removed %	moisture adsorbed mg	hydroc. adsorbed gmol/g
C9	25	1.1×10^{-7}	300	95	25	132×10^{-5}
C10	80	$.92 \times 10^{-7}$	330	96	15	164×10^{-5}
C11	100	$.31 \times 10^{-7}$	360	74	10	32×10^{-5}
C12	125	$.23 \times 10^{-7}$	345	60	2	23×10^{-5}

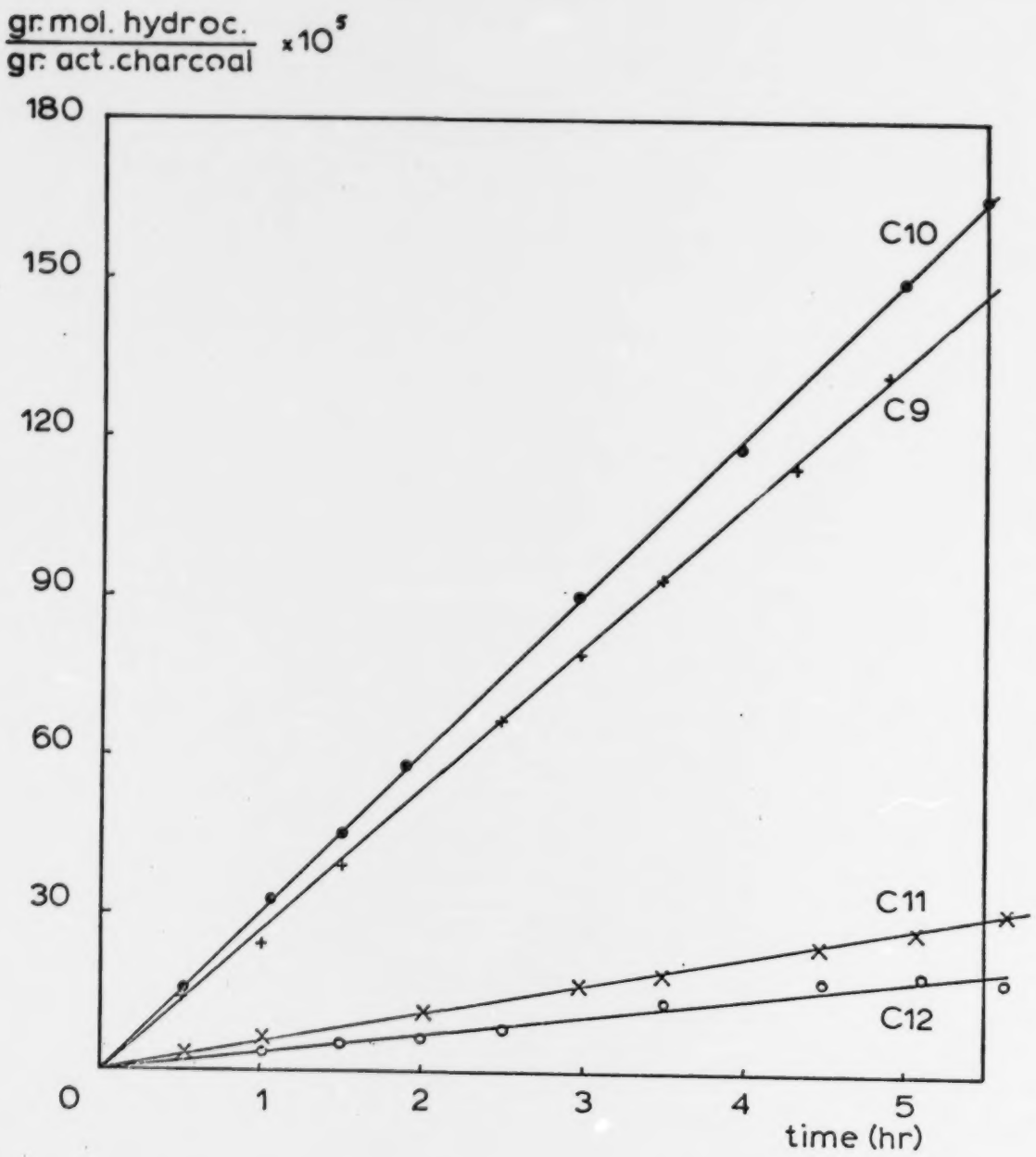

Figure 3.8. Effect of temperature on uptake.

- Too high a velocity will cause elutriation of the fluidized particles and create bubbles of gas which, in a shallow bed, will bypass the bed.
- Too low a velocity, even if it is high enough to create fluidization, will not insure a good mixing of the particles.

A definition for the minimum fluidization velocity was given in Section 2.2.2 and Eq. (2.13) allows for computing its value:

$$Re_p < 20 \quad u_{mf} = \frac{d_p^2 g(\rho_s - \rho_g)}{1650\ \mu} \tag{3.1}$$

Eq. (3.1) is appropriate because the particle Reynolds number has always been kept below 20. The minimum fluidization velocity was found to be 1.75 cm/s for the activated charcoal used, with particle diameters ranging between 270 μ and 350 μ.

This value is consistent with the values obtained by other investigators' correlations, for instance Rowe (6), Pinchbeck and Popper (7) and van Herden et al. [quoted by Wallis (9)].

Again, a definition of the terminal falling velocity is given in Sect. 2.2.2 and recalling Eqn. (2.17), the terminal falling velocity of the smallest particles present in the bed is

$$0.4 < Re_p < 500 \quad u_t = \left[0.0178 \frac{g^2(\rho_s - \rho_g)}{\rho_g\ \mu}\right]^{1/3} dp \tag{3.2}$$

which gives a value of 97 cm/s.

On average, the experimental fluidization velocity was 10 to 20 cm/s, well below the terminal falling velocity of the fines and about 5 to 10 times the minimum fluidization velocity.

3.2.5 Height of the bed, feed concentration, particle diameter

In his M.S. thesis, Schulte (11) using statistical analysis was able to correlate the hydrocarbon removal efficiency to the height of the bed, the inlet hydrocarbon concentration of the gas, the particle diameter, and the fluidization velocity.

His conclusions were:

- the hydrocarbon removal efficiency increases with increasing bed height; this is supported by the work of Richardson and Bakhtiar (12) and mainly due to the increase of available surface area of the catalyst.
- the hydrocarbon removal efficiency increases with increasing hydrocarbon concentration as a direct result of the increased driving force for mass transfer.
- the particle diameter has an optimal value since the smaller the particle the higher the surface area, but the more elutriation will take place.
- the same analysis holds for the fluidization velocity since the higher the velocity, the more intimate the gas solid contact, but the more elutriation and bubbles. The effect of bubbles has been discussed in Section 2.2.5.

3.3 Materials and specifications, setting of parameters

3.3.1 Materials and specifications

The experimental apparatus (see Fig. 3-1) is built with 304 stainless steel tubing, 3/8 in. in outside diameter, using Swadgelok connections.

The compressed air of "medical purity" containing less than 5 ppm

of hydrocarbon and less than 3 ppm of water vapour, was provided by Ohio Medical, Inc.

The compressed helium came from Air Reduction Company, Inc. and was of the quality "Oil Free".

The compressed hydrogen was also supplied by the same company and had less than 1 ppm oxygen, with a dew point of -81°F.

The analytical gas chromatograph is made by Carle Instrument Company, Inc. (Fullerton, Ca), model AGC 311.

The recorder is a 2-channel strip chart recorder supplied by Hewlett-Packard (model HP 7100 B).

The temperature controller is a Cole Parmer model 2155.

The chromatograph columns are two 6 ft-columns provided by Supelco (Bellefonte, Pa) packed with 10% SP-2100 on 100/120 Supelcoport No. 1-2465. They were chosen for their excellent ability to separate high boiling point hydrocarbons.

The hydrocarbon used is a n-tetradecane $CH_3-(CH_2)_{12}-CH_3$. It was provided by Eastman Kodak Co., and had the following properties: minimal purity = 98%, molecular weight = 198.39, melting point = 6°C, boiling point = 252°C; the vapour pressure vs temperature curve is presented in Fig. 3-9 (1.33×10^{-2} mm Hg at 20°C).

The activated charcoal was made by Westvaco, grade "Nuchar Activated Charcoal," crushed from 4 x 10 mesh, then sieved to the desired mesh. It had a surface area (Nitrogen B.E.T. method) of 850 m^2/g, and the bulk of pore volume was due to those pores with radii between 10 and 60 Å. The pore distribution is given in Fig. 3-10 (Ref. 11).

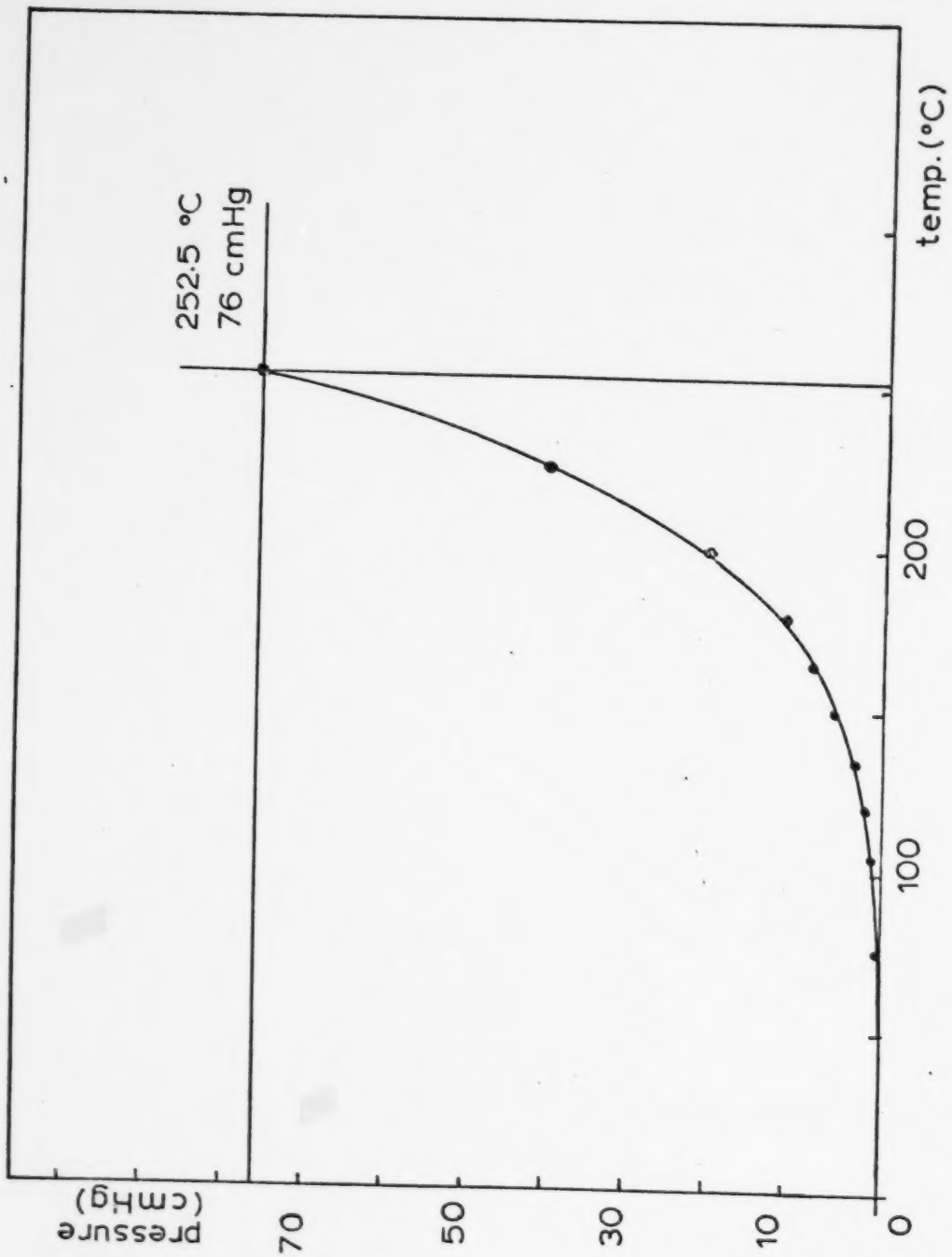

Figure 3.9. n-tetradecane vapor pressure vs temperature.

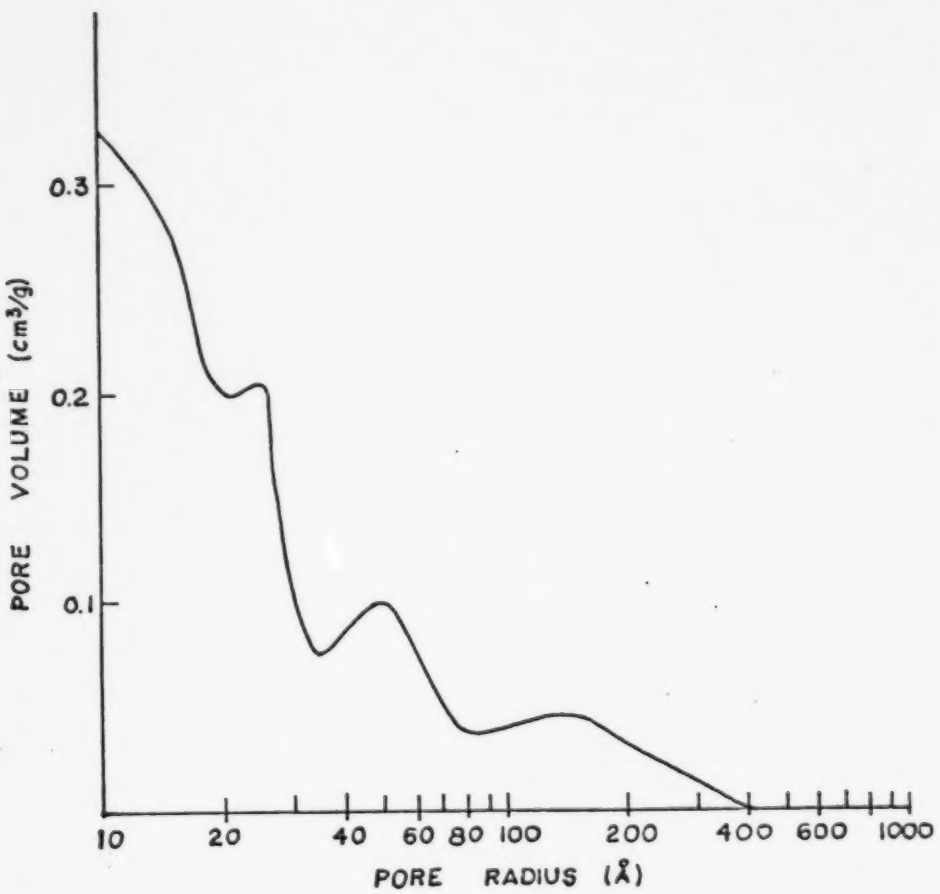

Figure 3-10. Charcoal pore-size distribution.

The activated alumina used in preliminary experiments came from ALCOA Chemicals.

An analytical balance was also used, built by Mettler, "S/P" model H31, sensitive to 10^{-4} gram.

The fluidized bed was a 1.25 in I.D. glass tube; the gas distribution was done by a sintered glass disk as represented in Fig. 3-11.

The hydrocarbon saturator was a stainless steel cylinder 3 in. in diameter and 2 ft high containing a 2 in. diameter sintered glass disk for gas distribution.

The water saturator was a column 2 in. in diameter by 2 ft high also containing a 1.5 in. diameter sintered glass disk for gas distribution.

3.3.2 Setting of the parameters

The gas chromatograph parameters were always set at the same value to insure the reproductibility of the experiments. They were:

- gas flow rates: Helium: 40 ml/min (20 per column)
  Hydrogen: 20 ml/min
  Air: 400 ml/min (all measured at STP)
- temperature of the columns: 200°C
- sensor : Falme Ionization Detector

The other parameters were allowed to vary within a controlled range:

- temperature of the bed: room temperature to 125°C
- mesh size of the carbon: 40 to 80 mesh
- total gas flow rate: 4.5 to 6.0 l/mn
- inlet hydro-concentration: 100 to 800 ng/cm^3
- mass of activated charcoal: 0.2 to 1.0 gram.

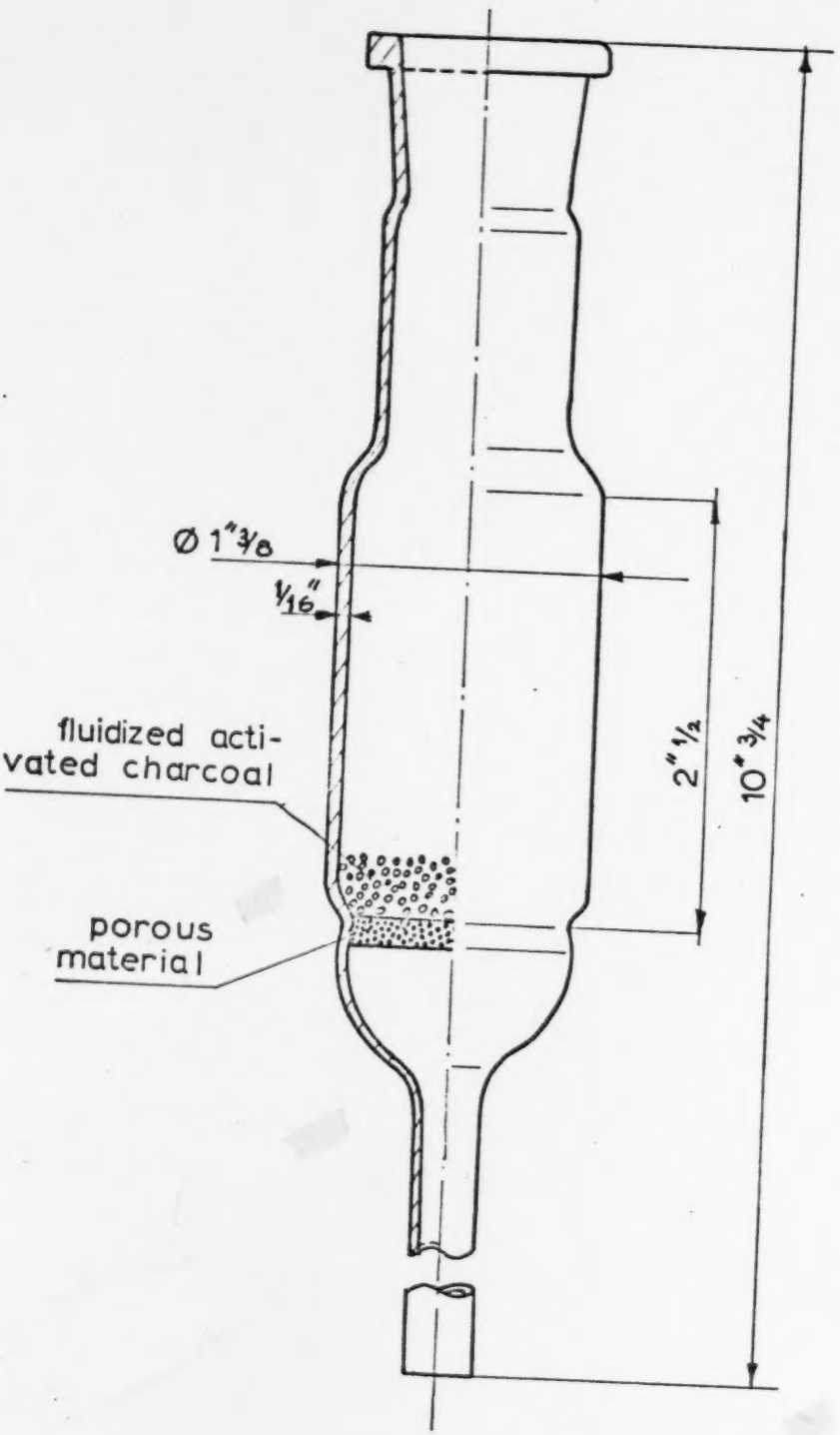

Figure 3-11. Sketch of the fluidized bed.

4. RESULTS AND MATHEMATICAL MODEL

4.1 Results

4.1.1 Measurement of the isotherm

The optimal operating temperature was found to be 80°C (see Section 3-2.2). Thus, the adsorption isotherm has to be accurately determined for this temperature.

There are two readily available ways of drawing the isotherm:

i) knowing that 6 to 8 particle diameters (10) into the bed, the gas is essentially in equilibrium with the solid, it is possible to carry out an experiment using a deep fluidized bed, temperature controlled at 80°C, for which increasing feed and corresponding outlet gas concentrations are recorded. The results of this method (experiment C14) are shown in Fig. 4-1.

ii) The second available method uses a gas chromatograph column packed with the charcoal used in the study (48). This column is installed in the gas chromatograph, with the temperature set at 80°C. A calibration of the apparatus is then necessary (the procedure is given in Appendix A). The results of this method are supposed to be more accurate, but performing this experiment is very difficult; obtaining one point requires about three hours, the n-tetradecane has to be diluted to 1 part per 100 (in toluene, for instance), and only very small amounts of this mixture may be injected (in the order of 1 nanoliter) in order to get results in the investigated range of concentration. A few points were determined by this method which are also shown on Fig. 4-1; both methods seem to agree.

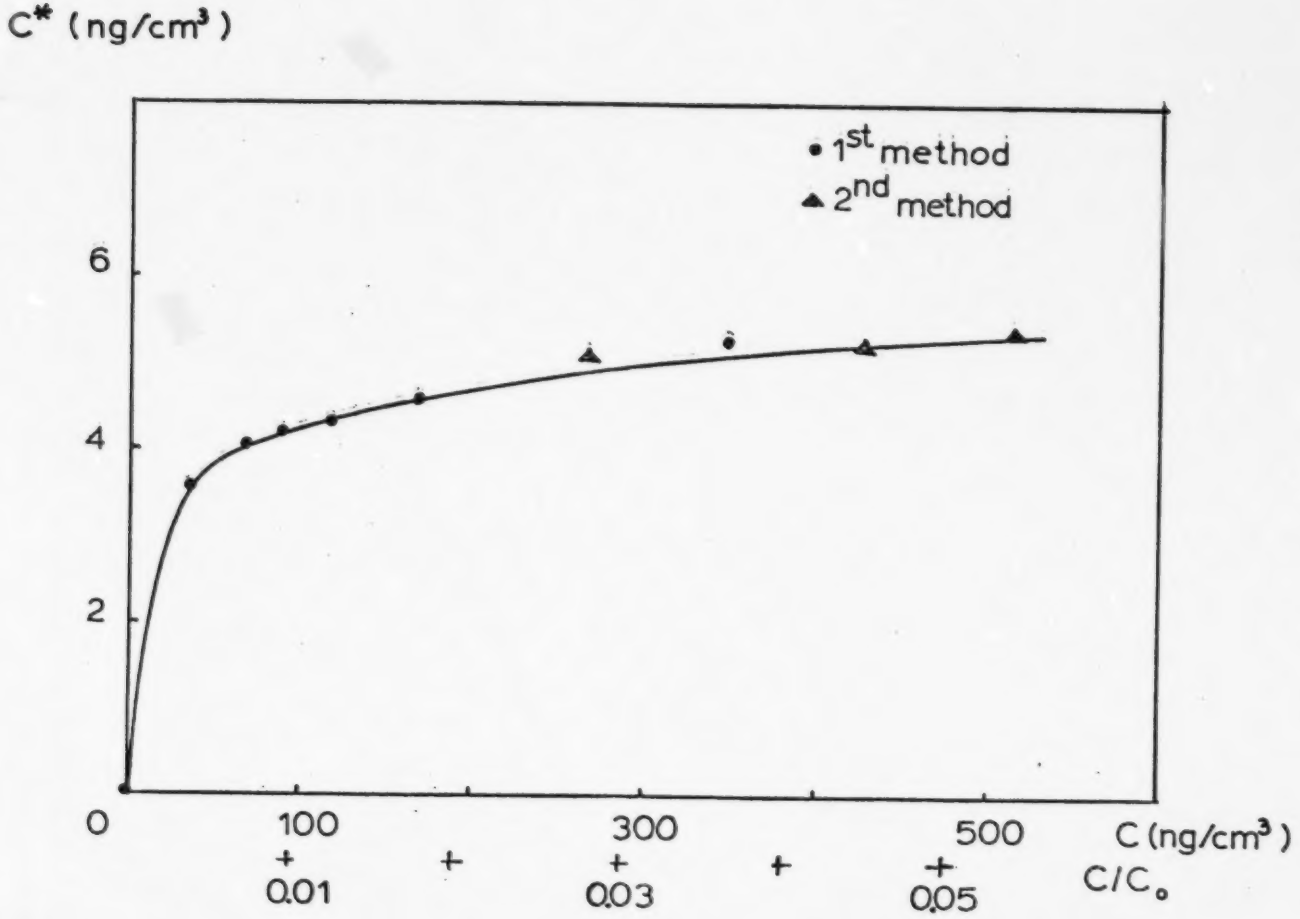

Figure 4-1. 80°C-isotherm of adsorption of n-tetradecane on activated charcoal.

It is interesting to increment the isotherm in terms of C_g/C_{g_o}, where C_{g_o} is the concentration corresponding to hydrocarbon saturation in the gas phase.

Knowing from Fig. 3-9 that, at 80°C, the saturation pressure is 1 mmHg, this saturation concentration is readily obtained by writing the gas equation of state:

$$\frac{n}{V} = \frac{p}{R\,T}$$

with

$$p = 1 \text{ mmHg} = 133 \text{ pascal}$$

$$R = 8.32 \text{ J/K}$$

$$V = 1 \text{ m}^3$$

$$T = 353 \text{ K}$$

$$\frac{n}{V} = C_{g_o} = 45.3 \times 10^{-9} \text{ mol/cm}^3 = 9.0 \times 10^{-6} \text{ g/cm}^3$$

The investigated range of concentrations is 50×10^{-9} to 500×10^{-9} g/cm^3 corresponding to C_g/C_{g_o} ranging from 0.005 to 0.055. From (14), it seems justifiable to assume that only a monolayer coverage occurs on the solids.

4.1.2 Analysis of a typical experiment

The following experiment (C17) (Fig. 4-2) was run to study the adsorption of n-tetradecane in the fluidized bed of activated charcoal in the presence of moisture, and is considered to be typical of the study.

The parameters were set at the following values:

- inlet gas composition: n-tetradecane 2.5×10^{-7} g/cm^3

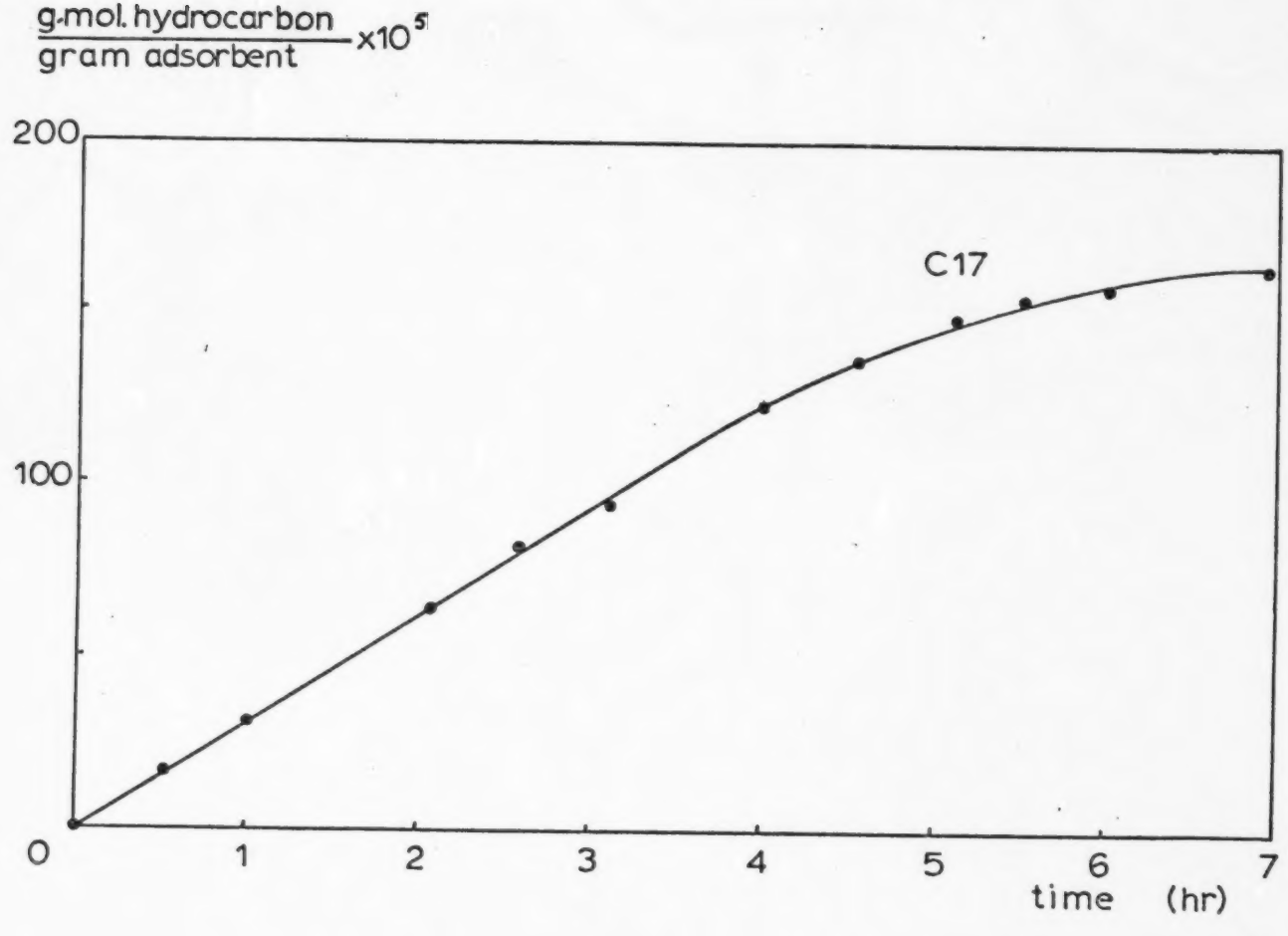

Figure 4-2. Typical adsorption run.

- saturated in moisture
- mass of charcoal: .6854 gram
- temperature of the bed: 80°C
- fluidization velocity: 9 cm/s

After the experiment was started, an almost linear increase in hydrocarbon uptake is recorded during the first 4 hours. The curve then tends to flatten and the rate of transfer decreases. The activated charcoal then reaches saturation which can be characterized by the appearance of channeling and slugging in the bed. The experiment was stopped at this point when most of the gas bypassed the adsorbent due to the poor quality of fluidization.

As can be deduced from the curve, the rate of mass transfer depends indeed on charcoal coverage; also, it can be estimated that the maximum adsorption ability of charcoal lies in the range of 150-160 x 10^{-5} g-mole of hydrocarbon/gram of adsorbent or about 300 g/kg of adsorbent. This can be confirmed from reference (25), where Hasz and Barrere recorded hydrocarbon uptakes on activated charcoal ranging from 20 to 220 g/kg of charcoal; the investigated hydrocarbons were paraffins ranging from C_2 to C_6 at 170°F under a partial pressure of 1 psi; also, it seems from their data, that this adsorption ability increases with increasing molecular weight.

4.1.3 Mass transfer coefficients

It has been suggested that mass transfer from the bulk of the gas to the solid takes place in three steps which can be characterized as follows (Fig. 4-3):

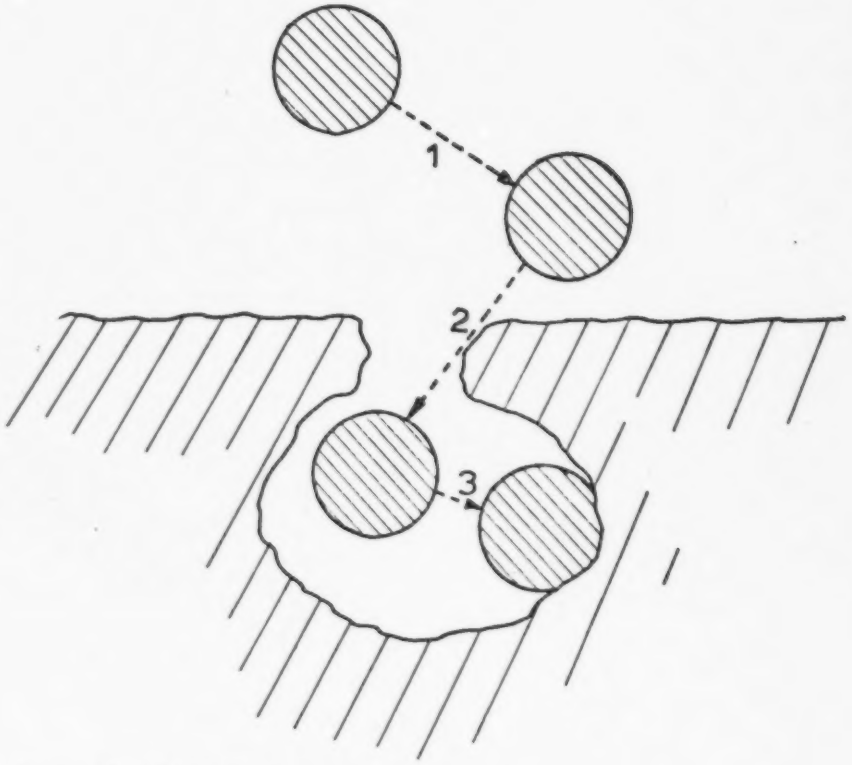

1 transfer through the gas film
2 — into the pore
3 — to the pore wall

Figure 4-3. Mass transfer controlling steps.

i) transfer of the hydrocarbon molecules through the gas film surrounding the particle

ii) transfer of the hydrocarbon molecules from the external surface of the carbon to the interior of the pore

iii) adsorption of the hydrocarbon molecules on the pore walls.

It is then possible to define the overall mass transfer coefficient as being:

$$K\,\Delta C_m = \frac{(C_g - C_p) + (C_p - C_s) + (C_s - C^*)}{1/K_G + 1/K_p + 1/K_a} \qquad (4.1)$$

where

K is the overall mass transfer coefficient

K_G is the rate coefficient for the transfer through the gas film

K_p is the rate coefficient for diffusion into the pores

K_a is the rate coefficient of adsorption

ΔC_m is the transfer mean driving force

C_g is the hydrocarbon concentration in the bulk of the gas

C_p is the hydrocarbon concentration at the external surface of the particle

C_s is the hydrocarbon concentration at the pore wall

C^* is the hydrocarbon concentration in equilibrium with the solid (from isotherm)

Romero and Johnson (26) developed a correlation between Froude and Reynolds numbers which can define the fluidization quality:

$$Fr \times Re_p \frac{(\rho_s - \rho_g)}{\rho_g} \frac{d_p}{d_c} \qquad \begin{matrix} <100 \text{ particulate} \\ >100 \text{ bubbling} \end{matrix} \qquad (4.2)$$

where the Froude number, Fr, is equal to $\frac{V_{mf}^2}{g\, d_p}$

ρ_s and ρ_g are the solid and gas density, respectively

d_p and d_c are the particle and column diameter, respectively.

When applied to the system investigated, the correlation has a value of .5, so that the presence of bubbles can be neglected and no gas bypasses the bed.

Perfect solid back mixing is assumed as was stated in Section 2.2.4.1.

The rate of mass transfer is expressed by:

$$\frac{\Delta N}{\Delta t} = K\, A\, \Delta C_m \qquad (4.3)$$

where

ΔC_m is the mean driving force for mass transfer

A is the available surface of the charcoal in the bed

The expression for the driving force depends on the gas flow pattern. Many gas flow patterns have been suggested, as is evident from the large variation of results reported in the literature. However, two extreme cases limit the gas flow patterns: perfect gas backmixing or piston flow pattern.

The driving force for mass transfer lies between the two following limits:

$$\Delta C_m = C_e - C^* \quad \text{(if gas backmixing is assumed)} \qquad (4.4)$$

$$\Delta C_m = \frac{C_f - C_e}{\ln \frac{C_f - C^*}{C_e - C^*}} \quad \text{(if piston flow is assumed)} \qquad (4.5)$$

4.1.3.1 Overall mass transfer coefficient assuming gas piston flow pattern

It has been suggested by an early investigator (10) that, in a fluidized bed, mass transfer is quite fast and after 6-8 particle diameter into the bed, the gas is essentially in equilibrium with the solid. This implies that, above 6-8 particle diameters, C_e is not significantly different from C^* and the resulting value of ΔC_m (Eq. 4.5) is much lower than the actual actual value of the driving force.

In order to overcome this difficulty, two experiments were carried out at 80°C using very shallow fluidized beds of activated charcoal, with depths less than the above critical value (see Fig. 4-4). The continuously changing slope of the curve gives a good indication that equilibrium was not reached.

Written in a finite difference form, the equation giving the mass transfer coefficient is now given by:

$$K = \frac{\Delta N}{\Delta t} \frac{1}{A} \frac{1}{\Delta C_m} \qquad (4.6)$$

When this equation is applied to experiments C15 and C16 for approximately zero coverage (after 1/2 hour), it gives the results in Table 4-1.

The values of K are not significantly different from each other. This is consistent with the fact that at zero coverage, the transfer of hydrocarbon through the gas film surrounding the particles is the limiting step and is not affected by the state of the system.

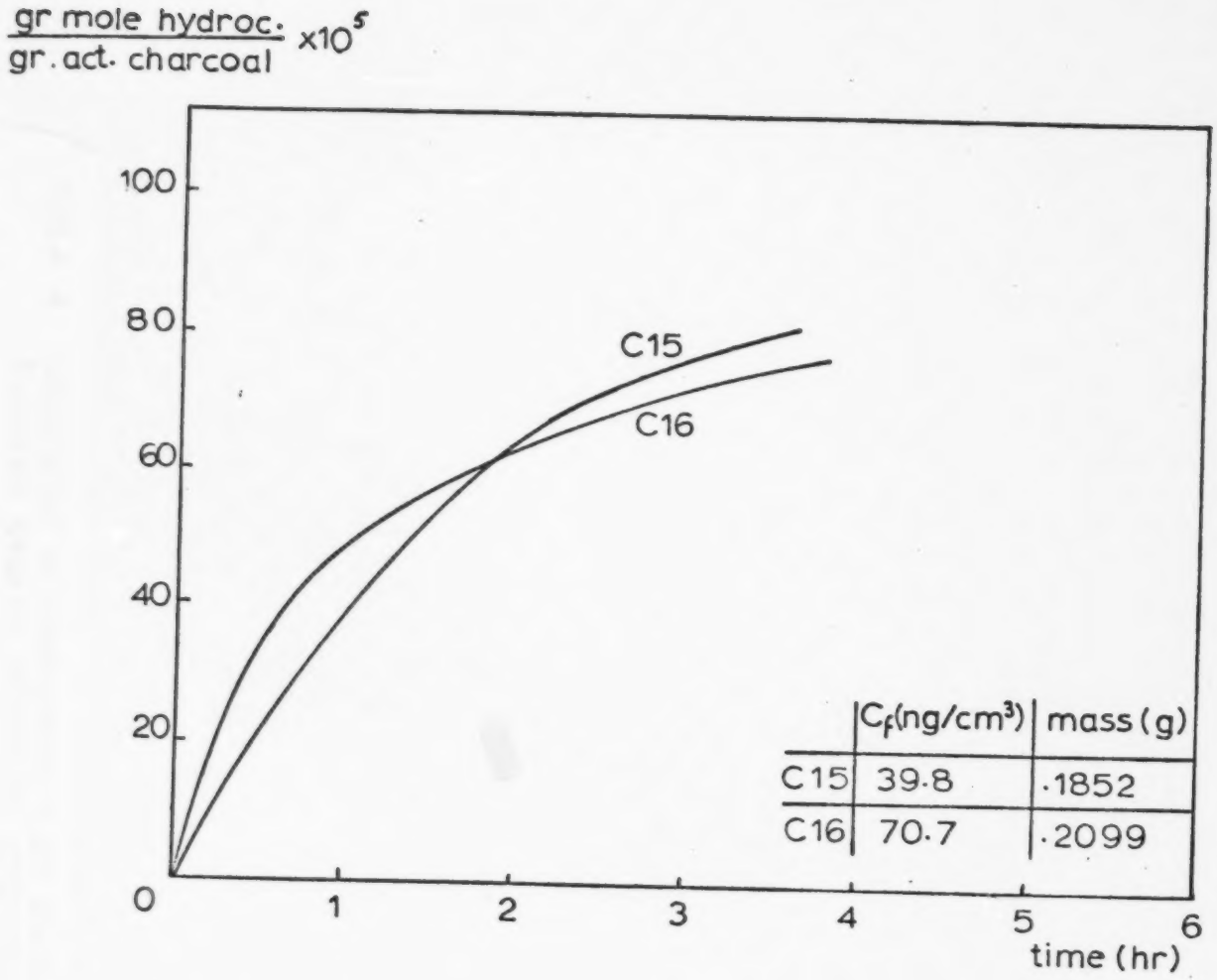

Figure 4-4. Adsorption of n-tetradecane on shallow fluidized beds of activated charcoal.

TABLE 4-1. MASS TRANSFER COEFFICIENTS ASSUMING PERFECT SOLID BACKMIXING AND GAS PISTON FLOW PATTERN, AT 0 COVERAGE

Run	C_i (ng/cm^3)	C_e (ng/cm^3)	C^* (ng/cm^3)	ΔC_m (ng/cm^3)	$\Delta N/\Delta t$ ($\mu g/s$)	K (cm/s)
C15	39.8	5.4	3.0	12.6	12.5	3.5
C16	70.7	8.4	3.9	23.0	20.6	3.2

4.1.3.2 Overall mass transfer coefficient assuming complete mixing of the gas

Under these conditions the assumption made is that the gas concentration is the same everywhere in the bed, and is equal to the outlet gas concentration. The driving force is given by Eqn. (4.4) and the results are shown on Table 4-2.

The values of the mass transfer coefficients are somewhat higher than in the former case since the calculated driving force is lower.

4.1.4 Mass transfer correlations

Many correlations have been derived to represent mass transfer. The Reynolds, Sherwood, and Schmidt numbers are very often used to represent such relationships.

Szekely (15) proposed the following expression:

$$Sh = .374\ Re^{1.18} \qquad 2 < Rep < 15 \qquad (4.7)$$

to represent the adsorption of carbon tetrachloride on activated charcoal. It seemed justified to test the above coefficients against this correlation in which

$$Sh = \text{Sherwood number} = \frac{Kd_p}{D}$$

$$Re = \text{Reynolds number} = \frac{\rho_g v d_p}{\mu}$$

μ is the viscosity of the gas

ρ_g is the density of the gas

D is the diffusivity of the hydrocarbon in the gas

v is the gas velocity

d_p is the particle diameter

TABLE 4-2. MASS TRANSFER COEFFICIENTS ASSUMING PERFECT SOLID BACKMIXING AND PERFECT GAS BACKMIXING AT ZERO COVERAGE

Run	C_i (ng/cm^3)	C_e (ng/cm^3)	C^* (ng/cm^3)	C_m (ng/cm^3)	$\Delta N/\Delta t$ ($\mu g/s$)	K (cm/s)
C15	39.8	5.4	0.5	4.9	12.5	9.0
C16	70.7	8.4	1.1	7.3	20.6	8.9

D can be approximated from the equation developped by Hirchfelder, Curtiss, and Bird quoted by (11):

$$D = 0.0018583 \frac{\sqrt{T^3(1/M_a + 1/M_b)}}{p\ \sigma_{ab}\ \Omega_{ab}} \qquad (4.8)$$

where

T is the temperature in °K

p is the absolute pressure in atm.

M_a, M_b are the molecular weights of components a and b, resp.

Ω_{ab} is the collision integral

σ_{ab} is the collision diameter in Å

Eqn. (4.8) gives a value of diffusivity of 3.50×10^{-2} cm^2/s. It is then possible to compute both Sherwood and Reynolds numbers to form the results in Table 4-3.

The experimental points show satisfactory agreement with Eqn. (4.7), especially those points computed for the gas piston flow assumption, as can be seen in Fig. 4-5. However, it has to be emphasized that the value of diffusivity is not very accurately known, which could make the Sherwood number vary within a certain range.

4.1.5 Comparison of the results

The results of this study differ slightly from Schulte's conclusions about the values of the overall mass transfer coefficients and the nature of the gas flow pattern, although the investigated systems were very similar. Schulte found that the gas flow pattern was more likely to be perfect gas backmixing with mass transfer coefficients of the order of 5 cm/s.

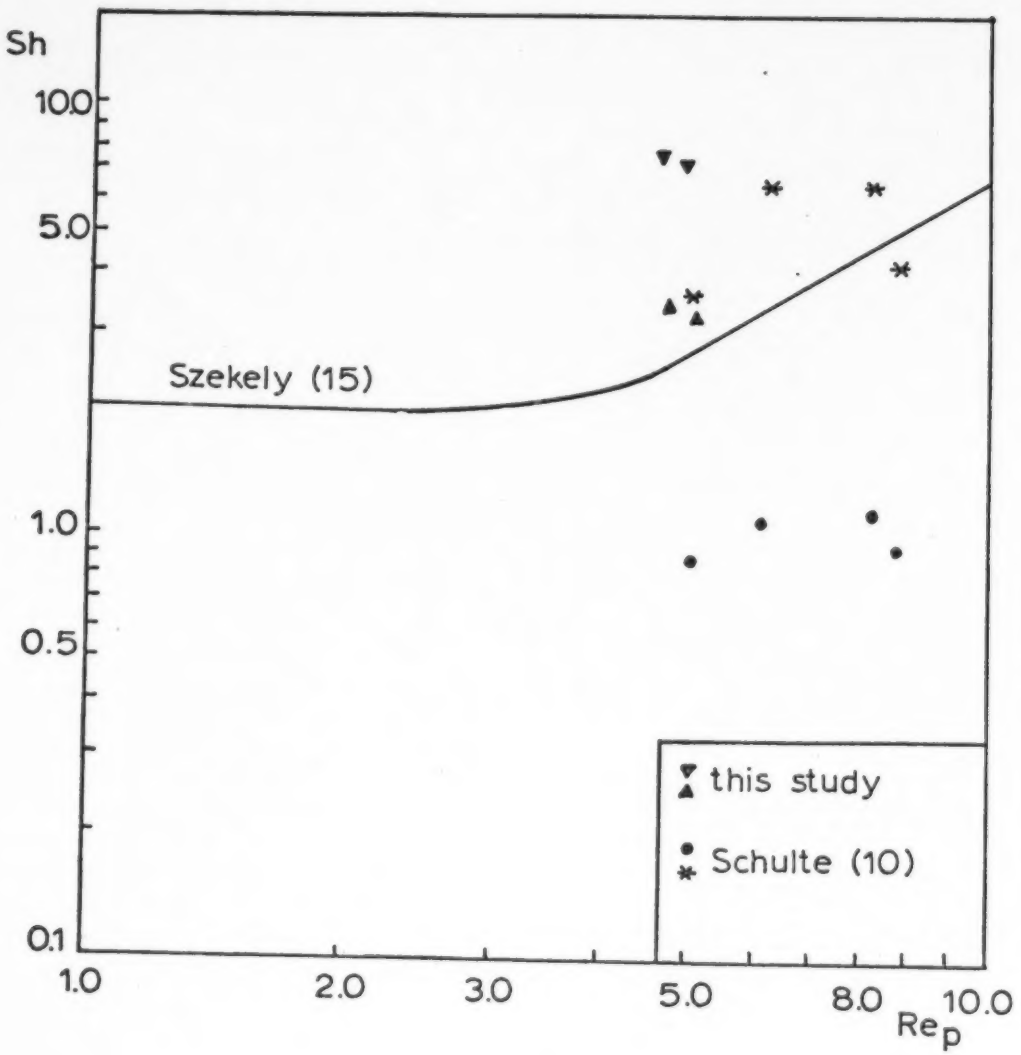

Figure 4-5. Plot of Re_p vs Sh and comparison with the results of other investigators.

TABLE 4-3. CALCULATED SHERWOOD AND REYNOLDS NUMBERS ASSUMING GAS PISTON FLOW PATTERN, THEN COMPLETE GAS MIXING

	run	K	u	Sh	Rep
piston flow	C15	3.5	6.81	3.0	5.0
	C16	3.2	7.2	3.1	5.2
Backmixing	C15	9.0	6.8	8.9	5.0
	C16	8.9	7.2	8.8	5.2

There were however, three differences in the approach to the results:

- Schulte conducted his experiments at room temperature and the results of this study are given for a bed temperature of 80°C; the hydrocarbon uptake has been found to be influenced by temperature (see Section 3.3 and Fig. 3-8), as is the hydrocarbon diffusivity.

- Schulte used a gravimetric method and recorded the weight increase of the bed to get his data. For adsorbent weight of about .6 g, the weight increase between two measurements taken 30 min. apart is of the order of 15 mg at most. This should be compared to the amount of the atmospheric moisture which is inevitably adsorbed on the sample when removed from the apparatus, brought to the balance, weighed and reinstalled in the apparatus. Fig. 4-6 shows the kinetics of moisture adsorption on activated charcoal and, as can be seen, a 5 min. exposure to the atmosphere will result in a weight increase of about 3 mg. Thus an error of 20% will result.

- Some of Schulte's experiments were conducted in deep beds (more than 6-8 particle diameters). And under these conditions it was difficult to obtain accurate values of the driving force.

4.2. Mathematical model

The mathematical model is based on the mass balance of both solid and gas phases in a controlled volume of thickness dz (see Fig. 4-7), under the basic assumption of no radial dispersion.

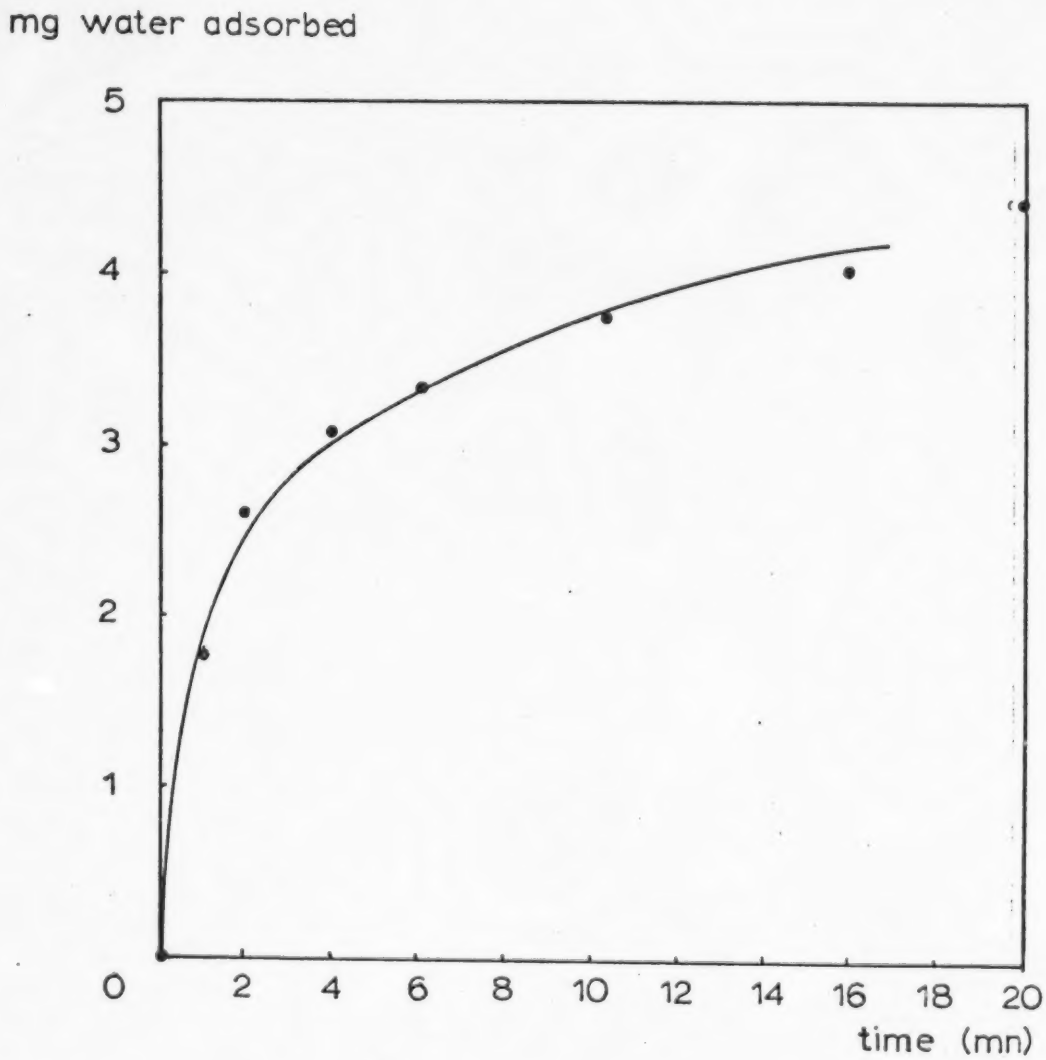

Figure 4-6. Adsorption of water on activated charcoal.

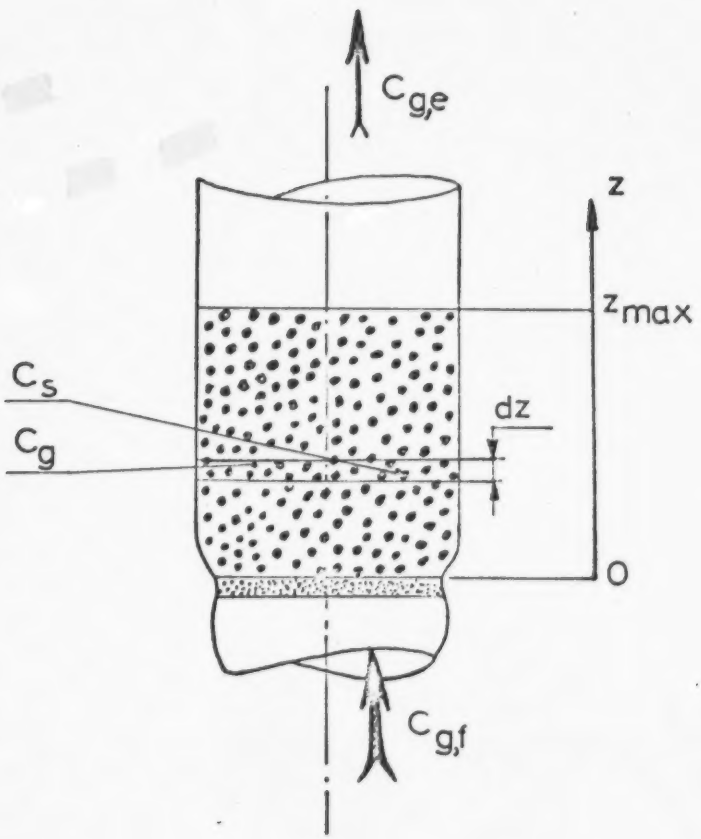

Figure 4-7. Definition of the coordinates for mass balance establishment.

4.2.1 Solid phase

It can be written for the solid phase:

rate of accumulation in the contr. volume	=	rate at which hydrocarbon is adsorbed	-	rate at which hydrocarbon is desorbed	(4.9)

Calling C_s the hydrocarbon concentration in the solid phase, which can depend on both spatial position, z, and time, t, the rate of accumulation can be written

$$(1 - \varepsilon)\ A\ \rho_s\ dz\ \frac{\partial C_s}{\partial t} = \text{rate of accumulation} \qquad (4.10)$$

where

A is the cross sectional surface of the bed

ε is the void fraction

ρ_s is the solid density

dz is the thickness of the control volume

Assuming the Langmuir monolayer adsorption hypothesis, the rate at which hydrocarbon is adsorbed on the activated charcoal is proportional to the available uncovered fraction $(1 - \theta)$, and the gas concentration (12). Then

$$\text{rate of adsorption} = [k_1\ C_g\ (1-\theta)\ A\ dz\ (1-\varepsilon)\ \rho_s]S_v \qquad (4.11)$$

where

k_1 is the foreward rate constant

C_g is the hydrocarbon concentration in the gas

S_v is the surface area of adsorbent per unit volume

Again, under Langmuir assumptions, the rate of desorption can be written:

$$\text{rate of desorption} = k_2\ \theta\ A\ dz\ (1-\varepsilon)\rho_s\ S_v \tag{4.12}$$

where

k_2 is the reverse rate constant

Substituting Eqn. (4.10) (4.11), and (4.12) into Eqn. (4.9) and simplifying, one obtains:

$$\frac{\partial C_s}{\partial t} = (k_1\ C_g(1-\theta) - k_2\theta)\ S_v \tag{4.13}$$

Equation (4.13) is the mass balance for the solid phase.

4.2.2 Gas phase

Similarly, for the gas phase, it can be written

rate of accumulation in the contr. volume	=	rate at which hydroc. enters the control volume	-	rate at which hydroc. leaves the control volume

$$+ \quad \text{rate of accumulation in the solid phase} \tag{4.14}$$

The rate of accumulation in the gas phase of the control volume can be expressed as

$$\varepsilon\ A\ dz\ \frac{\partial C_g}{\partial t} = \text{rate of accumulation} \tag{4.15}$$

The rate at which hydrocarbon leaves the control volume =

$$A\ V\ C_g^{z+dz} \tag{4.16}$$

The rate at which hydrocarbon enters the control volume =

$$A\ V\ C_g^{\ z} \tag{4.17}$$

where

V is the linear velocity of the gas.

By substituting Eqns. (4.15, 4.16, 4.17 and 4.13) in Eqn. (4.14) simplifying, and letting dz go to 0, one obtains

$$\varepsilon \frac{\partial C_g}{\partial t} = - V \frac{\partial C_g}{\partial t} - [k_1 C_g (1-\theta) - k_2 \theta] S_v \rho_s \ (1-\varepsilon) \tag{4.18}$$

The equations to be solved (Eqn. 4.3 and 4.18) form a system of two hyperbolic partial differential equations. Prior to computation it is customary to express these in a dimensionless form which is obtained by letting

τ be a dimensionless time: t/t_{max}

ξ be a dimensionless length: z/z_{max}

θ be a dimensionless concentration: C_s/C_s

ψ be a dimensionless concentration: $C_g/C_{g,f}$

The system of equations becomes:

$$\frac{\partial \theta}{\partial \tau} = t_{max} \frac{S_v}{C^*} (C_{g,f}\ k_1\ \psi\ (1-\theta) - k_2 \theta) \tag{4.19}$$

$$\frac{\partial \psi}{\partial \tau} = t_{max} \left[- \frac{V}{\varepsilon} \frac{1}{z_{max}} \frac{\partial \psi}{\partial \xi} - \frac{S_v}{C_s^*} \frac{1-\varepsilon}{\varepsilon} \rho_s \left(k_1\ \psi(1-\theta) - \frac{k_2}{C_{g,f}} \theta\right)\right] \tag{4.20}$$

The initial and boundary conditions may be described as follows: at $t<0$, the hydrocarbon concentration in the solid phase is zero everywhere in the bed, and for continuity, the hydrocarbon concentration in

the gas phase is equal to the feed concentration everywhere in the bed, the adsorption reaction not being allowed to take place. At t=0 the reaction takes place, and for t>0, and at z=0, the gas concentration is constant and equal to $C_{g,f}$.

C_s^* is the maximum hydrocarbon concentration in the solid phase, corresponding to the covered fraction = 1

$C_{g,f}$ is the feed concentration

t_{max} is the total duration of the experiment will equilibrium

z_{max} is the total length of the bed

In a dimensionless form, the initial and boundary conditions are written:

$$\tau < 0, \text{ for all } \xi, \quad \theta = 0 \tag{4.21}$$

$$\tau < 0, \text{ for all } \xi, \quad \psi = 1 \tag{4.22}$$

$$\xi = 0, \text{ for all } \tau, \quad \psi = 1 \tag{4.23}$$

4.3 Computer resolution of the mathematical modeling

4.3.1 Method

The method chosen was the 4th order Runge-Kutta method, which is very appropriate to solve such systems of partial differential equations (13). It uses a finite difference approach.

The partial differential equations must be written as follows

$$\left.\frac{\partial\theta}{\partial\tau}\right|_{\xi} = \frac{d\theta}{d\tau} = f_1(\tau, \xi, \theta, \psi) \tag{4.24}$$

$$\frac{\partial\psi}{\partial\tau} = f_2(\tau, \xi, \theta, \psi) \text{ at a given } \xi \tag{4.25}$$

Let's define the following quantities:

$h = \Delta\tau$ time increment

$$\begin{cases} a_{k_1} = h\, f_1(\tau, \theta, \psi) & (4.26) \\ a_{l_1} = h\, f_2(\tau, \theta, \psi) & (4.27) \end{cases}$$

$$\begin{cases} a_{k_2} = h\, f_1(\tau + \tfrac{1}{2}h, \theta + \tfrac{1}{2}a_{k_1}, \psi + \tfrac{1}{2}a_{l_1}) & (4.28) \\ a_{l_2} = h\, f_2(\tau + \tfrac{1}{2}h, \theta + \tfrac{1}{2}a_{k_1}, \psi + \tfrac{1}{2}a_{l_1}) & (4.29) \end{cases}$$

$$\begin{cases} a_{k_3} = h\, f_1(\tau + \tfrac{1}{2}h, \theta + \tfrac{1}{2}a_{k_2}, \psi + \tfrac{1}{2}a_{l_2}) & (4.30) \\ a_{l_3} = h\, f_2(\tau + \tfrac{1}{2}h, \theta + \tfrac{1}{2}a_{k_2}, \psi + \tfrac{1}{2}a_{l_2}) & (4.31) \end{cases}$$

$$\begin{cases} a_{k_4} = h\, f_1(\tau + h, \theta + a_{k_3}, \psi + a_{l_3}) & (4.32) \\ a_{l_4} = h\, f_2(\tau + h, \theta + a_{k_3}, \psi + a_{l_3}) & (4.33) \end{cases}$$

The fourth order Runge-Kutta method allows for writing:

$$\begin{cases} \Delta\theta^z = \frac{1}{6}(a_{k_1} + 2xa_{k_2} + 2xa_{k_3} + a_{k_4}) & (4.34) \\ \Delta\psi = \frac{1}{6}(a_{l_1} + 2xa_{l_2} + 2xa_{l_3} + a_{l_4}) & (4.35) \end{cases}$$

$$\begin{cases} \theta^z(\tau+h) = \theta^z(\tau) + \Delta\theta^z & (4.36) \\ \theta^z(\tau+h) = \psi^z(\tau) + \Delta\psi^z & (4.37) \end{cases}$$

4.3.2 Development of the computer program

The values of θ and ψ have to be computed for any location for a given time. This is readily done using the finite difference form

$$\left.\frac{\partial\psi}{\partial\xi}\right|_t = \frac{d\psi}{d\xi} = \frac{\psi_t^{z+1} - \psi_t^{z-1}}{2\Delta\xi} \qquad (4.38)$$

The purpose of the algorithm is to calculate both concentrations at a given time at any locations in the bed (increment J) and then move to the next time step (increment H). For this purpose, two (2 x JMAX) matrices are created, namely XO(I,J) (I = 1 is the concentration in the solid phase; I = 2 is the concentration in the gas phase, 1<J<JMAX) which represents the concentrations at time t, and X (I,J) (I = 1 is the concentration in the solid phase; I = 2 is the concentration in the gas phase, 1<J<JMAX) which represents the concentrations at time t + H.

$\Delta\theta^z$ and $\Delta\psi^z$ are computed at every ξ location following Eqn. (4.26) and (4.27), and XO(I,J) is related to X(I,J) through:

$$X(1,J) = XO\ (1,J) + \Delta\theta^z \qquad 1<J<JMAX \qquad (4.39)$$

$$X(2,J) = XO\ (2,J) + \Delta\theta^z \qquad 1<J<JMAX \qquad (4.40)$$

Because of the definition of the space derivative used (Eqn. 4.38), the above algorithm does not work at the boundaries $\xi = 0$ and $\xi = 1$. The first order Euler method is then used:

$$X\ (1,1) = XO(1,1) + H \times \left.\frac{\partial\theta}{\partial\tau}\right|_{\xi=0} \qquad (4.41)$$

$$X\ (1,JMAX) = XO\ (1,JMAX) + H \times \left.\frac{\partial\theta}{\partial\tau}\right|_{\xi=1} \qquad (4.42)$$

$$X\ (2,1) = 1 \text{ (boundary condition)} \qquad (4.43)$$

$$X\ (2,JMAX) = XO\ (2,JMAX) + H \times \left.\frac{\partial\psi}{\partial\tau}\right|_{\xi=1} \qquad (4.44)$$

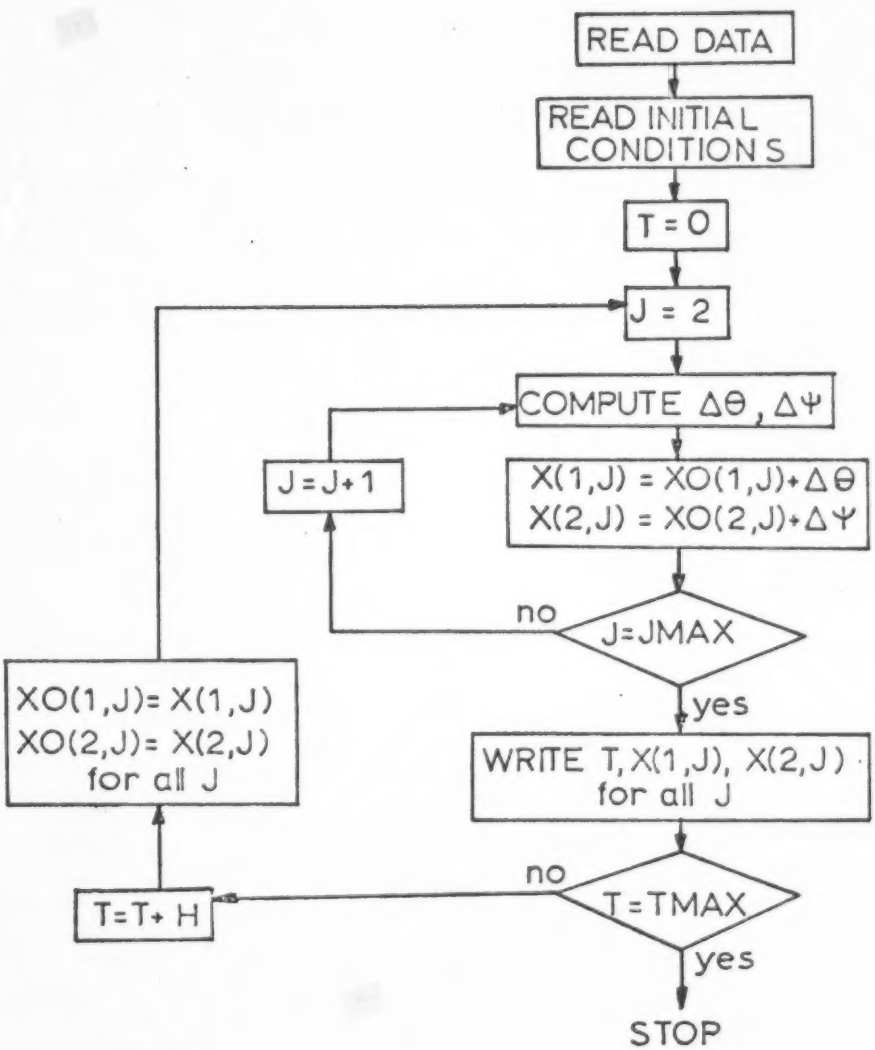

Figure 4-8. Computer flow chart.

A simplified flow chart for the program is shown in Fig. 4-8 and the detailed listing is given in Appendix B.

4.4 Validity of the model

The computer program was run using the following parameters:

- depth of the bed when fluidized: 5 mm
- air flow: velocity 10 cm/s
  hydrocarbon feed concentration $2.7\ mg/m^3$
- void fraction in the bed 0.65
- foreward rate constant 4.0 cm/s
- reverse rate constant $2 \times 10^{-7}\ kg/m^2/s$
- time increment 10^{-2} hr
- space increment 1.25 mm
- duration of the experiment 9 hr
- charcoal specific surface area $12400\ m^2/m^3$
- static density of the charcoal $600\ kg/m^3$
- maximum hydrocarbon uptake on charcoal 200 g/kg charcoal

The above conditions were very similar to chose of experiment C17 and a comparison of the experimental and computed results is given in Fig. 4-9. The calculated curve is the arithmetic average of the hydrocarbon concentration in the solid phase of the bed. As can be seen, the computed model fits rather well the experimentally obtained kinetics of hydrocarbon adsorption; the main characteristic of the experimental curves was the linear increase of the amount of hydrocarbon adsorbed which is well simulated. Also, the hydrocarbon concentration in the exit gas is also fairly well represented by the model (see Fig. 4-10): for 5 hours, the

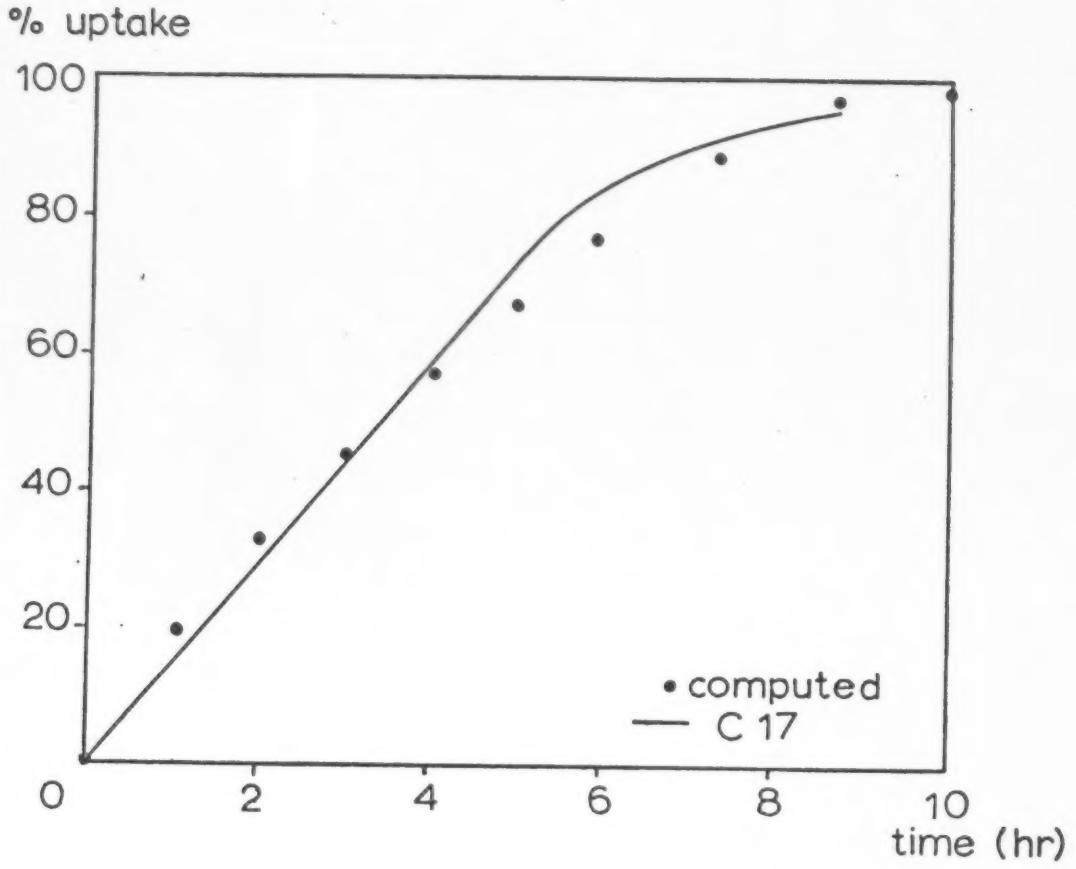

Figure 4-9. Validity of the mathematical model: solid phase.

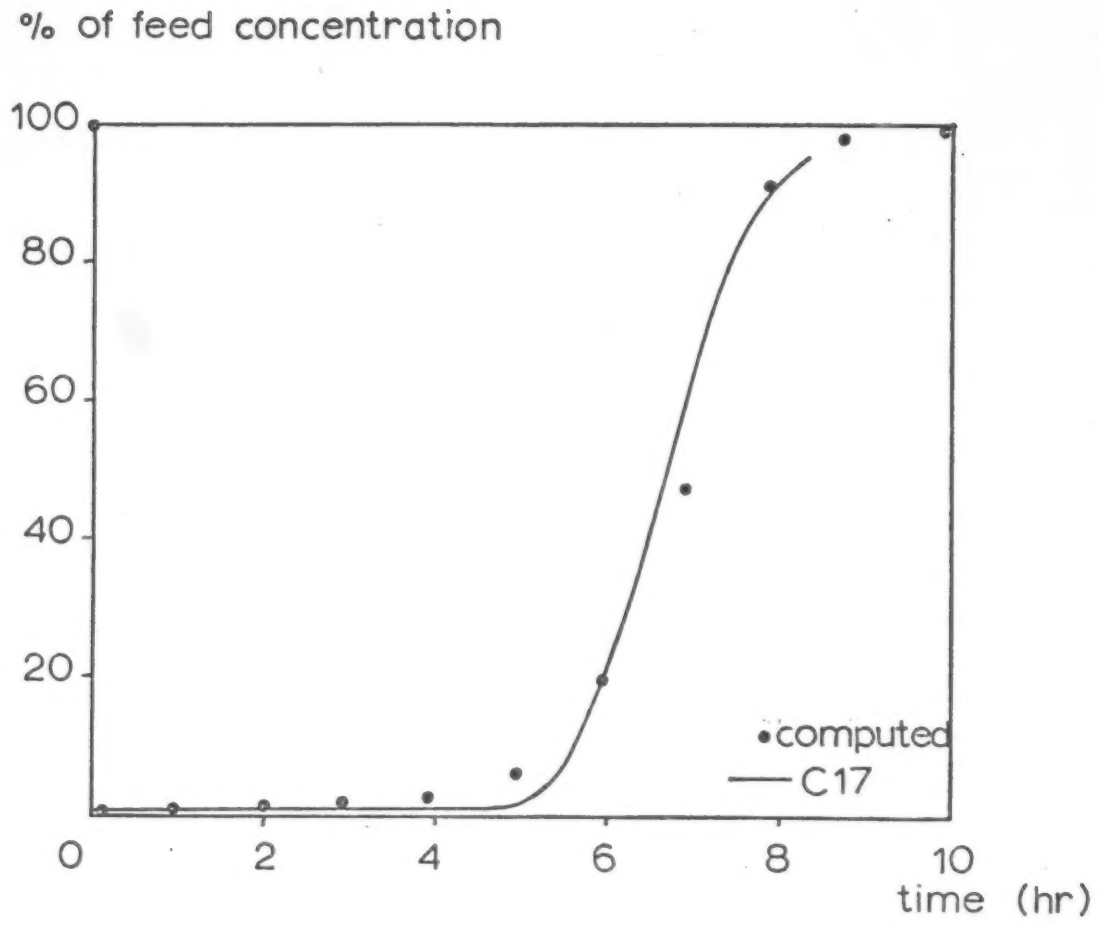

Figure 4-10. Validity of the mathematical model: gas phase.

bed has removed more than 90% of the hydrocarbon contained in the gas and this agrees with the experimental findings.

Note: Due to calculation stability requirements, the space increment to time increment ratio has to be lower than the value of the fluidization velocity. When expressed in the S.I. system the value of this velocity is rather low and since a shallow bed was modeled (small space increment) the time increment could not exceed a value of 10^{-3}s (simulating a ten hours long experiment would have required 3.6×10^{6} iterations or about 10 hours of IBM 1130 computer time).

In order to overcome this problem, the time has to be expressed in hours, but by doing so, the gas velocity would also have had to be expressed in m/hr which would have led to an even lower value of this velocity. The realization was made that the velocity term in the gas phase mass balance (Eqn. 4.18) occurs together with the hydrocarbon gas concentration and represents the hydrocarbon mass flux across the bed; instead of expressing the velocity in m/hr, the hydrocarbon feed concentration was actually multiplied by 3600; the foreward rate constant was expressed in m/hr and the reverse rate constant also had to be multiplied by 3600. By doing so, the time increment went up to 10^{-2} hr.

5. PRELIMINARY SCALE UP CALCULATIONS AND GENERAL CONCLUSIONS

5.1 Scale up calculations

In this chapter, two examples of scale up calculations will be briefly reviewed; since hydrocarbon vapors may be present in fugitive as well as point source emissions (see Section 1.2), the volume of the air to be processed and the concentration levels present may vary within a rather broad range.

5.1.1 Fugitive emissions

Fugitive emissions may occur in a sinterplant due to hydrocarbons produced from vaporization and cracking of lubricating oil. Briefly, sintering operations consist of agglomerating fine ore particles with coke at an elevated temperature before they can be used in steelmaking operations. Sinterplants are moving grates onto which the ore and coke particles are placed and then ignitied in the presence of excess air. This results in a narrow and high temperature flame front which, by traveling along the grate, produces the desired degree of agglomeration.

Assume a 50 m x 20 m x 6 m workshop with a hydrocarbon concentration of .2 ng/cm^3 of air and that the atmosphere has to be renewed every 5 hours. The air would then be passed through a fluidized bed of activated charcoal and, in order to make sure the bed would still be reactive enough, a maximum of 30% charcoal coverage by hydrocarbons is allowed.

It is then possible to dimension the fluidized bed and the charcoal consumption.

The flow rate is = 6000/5 Nm^3/hr = 0.334 Nm^3/s or 0.402 m^3/s at 80°C.

Assuming a gas linear velocity of 20 cm/s and a mean particle diameter of 300 μ, the conditions would very close to the experimental conditions (Re_p = 10.0 thus Sh = 5.0 and K = 5 cm/s).

The bed cross sectional area would be = .402/.2 = 2 m^2 and the diameter of the bed = 1.60 m.

If a bed depth of .03 m is assumed, the volume of charcoal present in the bed would be .06 m^3 corresponding to a mass of 36 kg.

Assuming a 30% coverage and a maximum removal capacity of 300 g/kg of charcoal, the adsorbent would have to be replaced for every 18,000 m^3 of gas passed through it or every 15 hours of continuous removal.

The charcoal consumption would then be 57.6 kg/day. It is interesting to compare this value with the results of Hutchins [quoted by Schulte (11)]. Hutchins investigated the regeneration of charcoal and found that if less than 350/400 lb/day is to be used, it would not be economical to regenerate the charcoal which would then be discarded.

Thus it is shown that for the type of application described above, a batch process would be efficient and profitable; installing a fluidized bed could also provide a means of controlling particulate pollutants in the workshop atmosphere, as well illustrated by the work of Zenz and Krockta (51).

5.1.2 Point source emissions

As defined in Section 1.2, point source emissions are the emissions which leave the plant through well defined routes and which are generally driven to the air cleaning plant for particulate removal. A report on pollution control in the Japanese steel industry (52) indicates that the flow rates handled in particulate removal devices are of the order of

50,000 Nm^3/hr to 1,000,000 Nm^3/hr. This dust free air which leaves the scrubbers and baghouses still contains, say, 0.5 gram of hydrocarbon per cubic meter of air which is the upper limit of the concentration range investigated in this study.

For instance, a flow rate of 60,000 Nm^3/hr will be considered (60,000 Nm^3/hr = 20 m^3/s at 80°C) corresponding to a sinterplant processing 1,000,000 tons of sinter/annum.

Typical particle size and nominal fluidization velocities used in industrial fluidized beds are as follows (53):

- particle size: normal distribution of sizes over the range of 30 mesh to 70 mesh
- fluidization velocity: ranging between 2.5 to 3.0 ft/s.

If a fluidization velocity of 2.5 ft/s is chosen, it will give for a Reynolds number of 5.0, a mean particle diameter of 200 μ, which is still close to the particle size used in this study.

The cross sectional area of the bed would then be = 22.3 m^2 corresponding to a bed diameter = 5.4 m. This figure is to be compared to the bed diameter in the Courtaulds process (see Fig. 2-4 and Ref. 32) which was found to be 30 ft or 10 m.

Again, assuming a 3 cm deep bed, the volume of activated charcoal would be 0.67 m^3 corresponding to a mass of about .4 tons. Allowing only a 30% coverage, the bed could remove 40.1 kg of hydrocarbon before having to be replaced. This mass of hydrocarbon corresponds to an operating time of 2 hours; in this case, charcoal regeneration would have to take place in situ.

In view of the order of magnitude of the bed diameter and time, and considering that larger fluidization velocities would enhance bubbling and bypassing of the gas, it would be reasonable to use a multistage adsorber, the diameter of which could be somewhat reduced. Furthermore, since the hydrocarbon removal would have to be fast indeed, a continuous countercurrent flow type process could be considered, as presented in Fig. 5-1.

This proposed process differs from the Courtaulds process by the addition of a drying vessel which is a necessary part of the charcoal regeneration (21). It is also known that elutriation problems would have to be taken into account (possibility of charcoal additions and wet scrubber for the off-gases, etc.) (23, 46).

5.2 Conclusions

It is hoped that this work can provide reliable information toward the realization of an economical process for hydrocarbon removal from steelplant effluent gases.

Seventeen experiments were run to study the adsorption kinetics of n-tetradecane onto a fluidized bed of activated charcoal. These experiments confirmed the feasibility of the proposed system and helped define the optimal operating conditions. They also proved that activated charcoal is able to remove hydrocarbon vapors in preference to water vapors when heated to 80°C.

Five more experiments were carried out using activated alumina instead of activated charcoal as an adsorbent. These showed that alumina has a stronger reactivity with water vapor than with hydrocarbon, and is not suitable for the system.

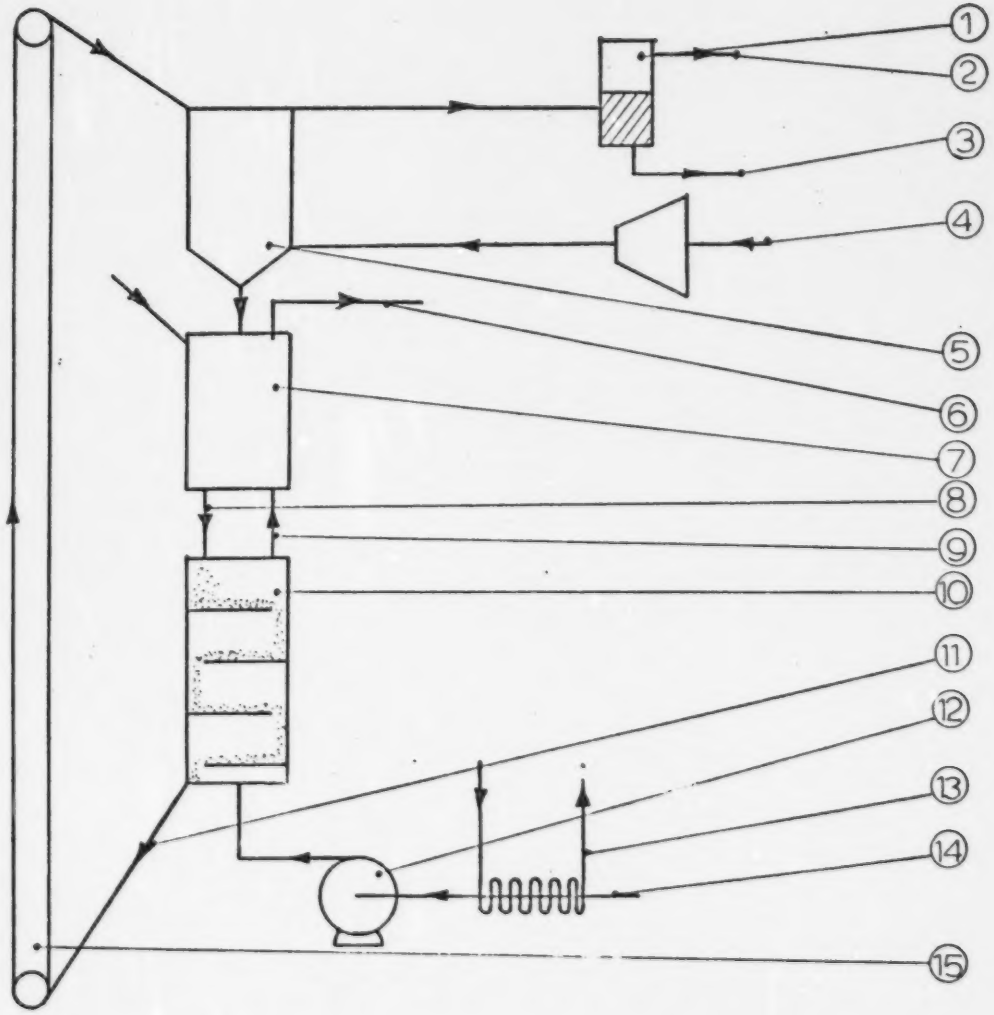

Figure 5-1. Possible flow chart of the proposed system.

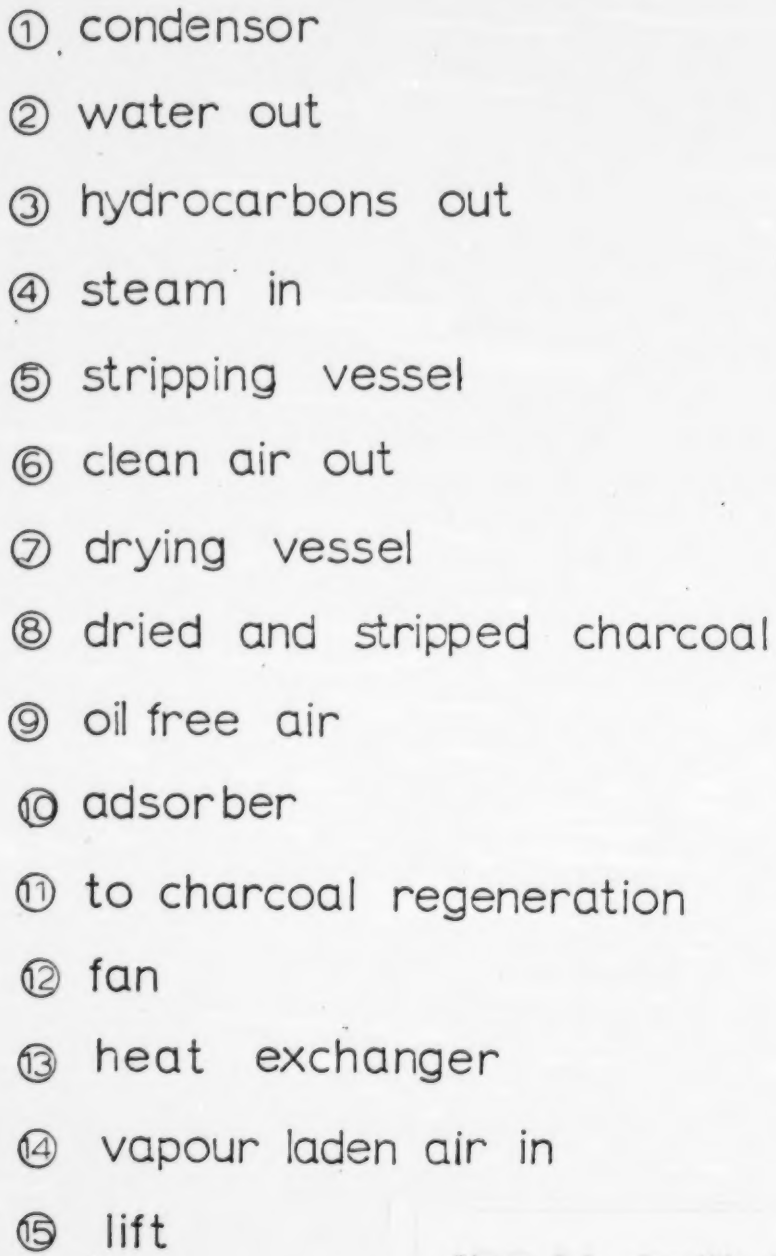

Figure 5-1. Possible flow chart of the proposed system.

The overall mass transfer coefficients were calculated and showed rather satisfactory agreement with Szekely's correlation (15) when perfect solid backmixing and gas piston flow pattern were assumed.

A mathematical model based on physical adsorption theory was derived and was found to give a satisfactory explanation of the kinetics of n-tetradecane adsorption on activated charcoal. The computed concentration profiles in both solid and gas phases were found to agree with experimental data.

Two case studies based on available data were briefly reviewed and the order of magnitude of the characteristic dimensions of the adsorbers were found to fall well within the limits of currently used industrial fluidized beds.

REFERENCES

1. H. Darnel, Engineering aspects of pollution control in the metal industry, Proc. of Int. conference held in London on 27-29 Nov. 1974, The Met. Soc. ed., 1975 .
2. K. R. Spring, Health and steel industry, the steel industry and the environment, J. Szekely ed., Marcel Dekker, New York, 1973.
3. J. Szekely, The environmental impact of the steel industry in developed nations, report to the United Nations Environmental Program presented in Geneva, Oct. 1978.
4. J. Szekely and N. J. Themelis, Rate phenomena in process metallurgy, John Wiley & Sons, New York 1971.
5. C. Y. Wen and Y.H. Yu, AIChE Journ. 12, 610, 1966.
6. R. N. Rowe and G. A. Henwood, Trans. Inst. Chem. Eng. vol. 39, p. 43 ,1961 .
7. P. H. Pinchbeck and F. Popper, Chem. Eng. Sc., vol. 1, p. 57, 1956.
8. D. van Heerden, A.P. Nobel and D. W. van Krevelen, Chem. Eng. Sc., vol. 1, p. 63, 1956.
9. G. B. Wallis, One dimensional two-phase flow, McGraw-Hills, 1969.
10. J. Szekely, J. W. Evans and H.Y. Sohn, Gas solid reactions, Academic Press, New York, 1976.
11. T. R. Schulte, The tertiary treatment for hydrocarbon removal from steelmaking effluents, M.S. thesis, State University of New York, Buffalo, April 1977.
12. R. A. Swalin, Thermodynamics of solids, John Wiley & Sons, New York, 1962.

13. R. L. Ketter and S.P. Prawel Jr., Modern methods of engineering computation, McGraw-Hill, New York, 1969.

14. C. N. Satterfield, Heterogeneous catalysis in Practice, M.I.T. Course 10.63: Adsorption and Catalysis, 1978.

15. J. Szekely, Mass transfer to porous solids in gas solid fluidized systems, Ph.D. thesis, Imperial College, London, 1961.

16. I. Langmuir, J. Am. Chem. Soc. 40, 1361, 1918.

17. S. Brauner, P.H. Emmer and E. Teller, J. Am. Chem. Soc., 60, 309, 1938.

18. A. J. Gonzales and C.D. Holland, AIChE J., 11, 1965.

19. A. J. Gonzales and C. D. Holland, AIChE J., 2, 470, March 1971.

20. J. J. Carburry, Chemical and catalytic reactions engineering, McGraw-Hill, 1976.

21. D. Kunii and O. Levenspiel, Fluidization engineering, John Wiley and Sons, New York, 1969.

22. R. H. Weyland, Fluidization technology, D. L. Keairns ed., McGraw-Hill, New York, 1976.

23. D. Merrick and J. Highley, AIChE Symp. Series, 137, vol. 70, p. 336, 1974.

24. C. Y. Wen and S. Dutta, AIChE Symp. Series, 161, vol. 74, 1978, p. 1.

25. J. W. Hasz and C. A. Barrere Jr., AIChE Symp. Series, 161, vol. 74, 1977, p. 1.

26. J. B. Romero and L. N. Johanson, AIChE Symp. Series, 38, vol. 58, 1962, p. 28.

27. J. R. Pfafflin, M. Shridhar and G. A. Jullien, AIChE, Symp. Series 105 vol. 66, 1970, p. 69.

28. W. B. Hartfield and N. R. Amundson, AIChE Symp. Series 116, vol. 67 ,1971 , p. 54.

29. J. R. Grace, ibid., p. 159.

30. T. Blickle, O. Borlai and L. Hodany, La fluidisation et ses applications, compte rendu du congrès Int., Toulouse 1973, Sté. Chimie Ind. ed., 1974, p. 73.

31. J. W. Hassler, Activated charcoal, Chemical Publishing Co., New York, 1963.

32. D. A. Avery and D. H. Tracey, Fluidization, Proc. of Symp. held on 24-25 Sept. in Montréal, Inst. of Chem. Eng. Symp. Series London , 1968 , p. 28.

33. H. Angelino, H. Gibert and H. Gardy, ibid., p. 67.

34. F. B. Smith and G. Brunet, AIChE Symp. Series 117 vol. 67 , 1971 , p. 58.

35. R. F. Mindrup Jr., Determination of organic vapors in industrial atmosphere, Bulletin 769A, Supelco Inc., Bellefonte Pa , 1977 .

36. United States Steel Corporation, The Making, Shaping and Treating of Steel, H.E. McGannon ed., 9th edition, 1971 p.172.

37. K. Yoshida and C.Y. Wen, AIChE Symp. Series, 116 vol. 67 , 1971, p. 151.

38. H. M. Rowson, Brit. Chem. Eng. 8, 180 , 1963 .

39. S. Elmaleh, J.L. Soulié and R. Ben Aim, La fluidisation et ses applications, Compte rendu du congrès Int. Toulouse 1973, Sté. Chimie Ind. ed. 1974.

40. N. N. Bakshi and A. Nihalani, ibid., p. 534.

41. J. G. Yates and J.A.P. Constas, ibid., p. 481.

42. J. F. Davidson and D. Harrison, Fluidized particles, Cambridge University Press, Cambridge, 1963.

43. S. Mori and C.Y. Wen, Fluidization technology vol. 1, D.L. Keairns ed., Hemisphere publ. Corp. Washington, 1976.

44. M. Tamalet, La fluidisation et ses application, Compte Rendu du congrès Int. Toulouse 1973, Sté. Chimie Ind. ed., 1974.

45. R. L. Bayers, J.W. Davis, W.L. Matson and H. A. McKinstry, AIChE Symp. Series, 137, vol. 70, 1974, p. 323.

46. W.K. Lewis, E.R. Guilliland and P.M. Lang, AIChE Symp. Series 38, vol. 58 (1962), p. 65.

47. E. D. Ermenc, Chem. Eng. 68, 87 ,1961.

48. A. V. Kiselev and Y.I. Yashin, Gas adsorption chromatography, transl. from Russian by J.E.S. Bradly ed., Plenum Press, New York 1969.

49. R.D. Fulker, Processes for air pollution control, G. Nonhebel ed., 2nd ed., Newnes-Butterworth, London 1972.

50. S. Ergun, Chem. Eng. Progr., 28, 89 , 1952.

51. F. A. Zenz and H. Krockta, Symp. Series, 116, vol. 67, 1971, p. 245.

52. The present status of environmental measures, report from Kimitsu Works, Nippon Steel Corp., 1975.

53. J. E. Hanway, Jr., AIChE Symp. Series, 116, 67, 1971, p. 244.

54. J. H. Perry, Chemical Engineering Handbook, McGraw-Hill, New York, 1963.

LIST OF SYMBOLS

a_k, a_l = symbols used in deriving the 4th order Runge-Kutta method

A = cross sectional area of the bed

B = constant in Eqn. (2.6)

c = constant in Eqn. (2.5)

C = hydrocarbon concentration

C^* = gas hydrocarbon concentration in equilibrium with the solids

C_s^* = maximum hydrocarbon uptake in the solid phase

ΔC_m = mean driving force for mass trnasfer

d = diameter

D = gas phase diffusivity

D_s = solid phase diffusivity

E = heat of reaction

E_s = solid diffusion coefficient

E_f = heat of adsorption for the first layer

E_1 = heat of adsorption

E_2 = heat of desorption

Fr = Froude number

F_g = gravity forces

g = acceleration due to gravity

h, H = time increment

ΔH = differential enthalpy of adsorption

I = integer

J = integer

K = mass transfer coefficient

k_1 = "foreward" rate constant

k_2 = "reverse" rate constant

k_{1_o}, k_{2_o} = constants in Eqn. (2.9)

L = height of the bed

m = mass

M = molecular weight

N = number of mole transferred

p = pressure

p_o = saturation pressure

ΔP = pressure drop across the bed

q_o = differential heat of adsorption

R = Boltzman's constant

Re = Reynolds number

Sc = Schmidt number

Sh = Sherwood number

S_v = charcoal surface area per unit volume of the bed

t = time

T = absolute temperature

u = linear gas velocity

$\dot{v}$ = gas volume flow rate

V = volume

V_m = volume of the first complete adsorbed layer

X(I,J) = (2 x JMAX) matrix

XO(I,J) = (2 x JMAX) matrix

z = length

Greek letters

α = constant in Eqn. (2.6)

ε = void fraction

Δ = finite increment

θ = covered fraction

μ = gas viscosity

ρ = density

σ = collision diameter

τ = dimensionless time

ϕ_s = shape factor

ξ = dimensionless length

ψ = dimensionless concentration

Ω = collision integral

Subscripts

a, ads = adsorbed

c = column

e = exit

f = feed

g = gas

G = transfer through the gas film

HC = hydrocarbon

i = inlet

L = liquid

mf = minimum fluidization

max = maximum

o = outlet

p = particle, pore

s = solid

APPENDICES

A. DETERMINATION OF THE ISOTHERM OF ADSORPTION USING THE AGC

B. COMPUTER LISTING AND RESULTS

C. CALIBRATION OF THE ROTAMETERS

APPENDIX A

DETERMINATION OF THE ISOTHERM OF ADSORPTION

Let us write the mass balance on a layer of adsorbed hydrocarbon:

$$-u_o\, v\, (\frac{\partial c}{\partial x})_t = v(\frac{\partial c}{\partial t})_x + v_a(\frac{\partial c_a}{\partial t})_x \qquad (A.1)$$

where

u_o is the linear velocity of the carrier gas

v volume of gas phase in the column

v_a volume of adsorbed layer

c concentration of adsorbate in the gas phase

c_a concentration of adsorbate in the adsorbed layer

t time elapsed from injection of the sample

x distance from start

Eqn. (A.1) can be written:

$$-u_o\, v(\frac{\partial c}{\partial t})_x (\frac{\partial t}{\partial x})_c = v(\frac{\partial c}{\partial t})_x + v_a(\frac{\partial c_a}{\partial c})_x (\frac{\partial c}{\partial t})_x$$

or

$$u_o\, v/(\frac{\partial x}{\partial t})_c = v + v_a(\frac{\partial c_a}{\partial c})_x \qquad (A.2)$$

in which $(\frac{\partial x}{\partial t})_c$ is the linear velocity at a point of given $c = u_c$ and $v_a(\frac{\partial c_a}{\partial c})_x$ is the slope of the adsorption isotherm at a point of given c. Noting that $(\frac{\partial c_a}{\partial c})_x = \frac{dc_a}{dc}$ and calling the uptake a, we have: $v_a dc_a = m\, da$ if m is the mass of adsorbent, and from (A.2):

$$\frac{da}{dc} = \frac{v}{m}(\frac{u_o}{u_c} - 1) = \frac{w}{m}(t_c - t_o) = \frac{V_c}{m} \qquad (A.3)$$

where

w is the carrier gas flow rate

t_c, t_o are the retention times for the adsorbate (at concentration c) and the carrier gas

V_c is the retained volume of adsorbate at concentration c.

Equation (A.3) is the equation of the adsorption isotherm:

$$a = \frac{1}{m} \int_o^c V_c dc \qquad (A.4)$$

We now have to express (A.4) as a function of the quantities recorded by the chromatograph recorder. The pen deviation of the recorder is proportional to c.

$$c = k \times h \qquad (A.5)$$

if h is the pen deviation and k is a given constant for given compound and sensitifity range.

Calibration of the apparatus:

By injecting an accurately known mass m', the exit composition is given as

$$m' = \int_o^\infty c' \, dV \qquad (A.6)$$

with,

if q is the chart speed: $q = \frac{dz}{dt}$ (A.7)

and

$$w = \frac{dV}{dt} \qquad (A.8)$$

Eqns. (A.7) and (A.8) give:

$$dV = \frac{w}{q} dz \qquad (A.9)$$

Substituting Eqns. (A.5) and (A.9) in (A.6) gives:

$$m' = k \frac{w}{q} \int_o^\infty h' \, dz = k \frac{w}{q} S' \qquad (A.10)$$

where S' is the area of the peak corresponding to m'.

The calibration constant is thus:

$$k = \frac{m'q}{S'w} \tag{A.11}$$

remembering that

$$V_c = w\,(t_c - t_o) = \frac{w}{q}\,(z_h - z_o)$$

if $z_h - z_o$ is the distance on the chart from the point of emergence of an unadsorbed component to the point where gas of concentration c (deflection h) occurs, then from Eqn. (A.4)

$$a = \frac{kw}{mq}\int_o^h (z_h - z_o)\,dh = \frac{kw}{mq}\,S_a \tag{A 12}$$

where S_a is the area on the chart between the axis o h at $z = z_o$ nd the edge of the peak.

Substituting Eqn. (A.11) into Eqn. (A.12) gives

$$a = \frac{m'\,S_a}{m\;S'} \tag{A.13}$$

It follows from Eqn. (A.11) that the c corresponding to a is:

$$c = \frac{m'\,q\,h}{S'\,w} = kh \tag{A.14}$$

Plotting a vs c will give the adsorption isotherm.

APPENDIX B

THE COMPUTER PROGRAM

```
PAGE   1

// JOB T

LOG DRIVE   CART SPEC   CART AVAIL  PHY DRIVE
  0000        08CE        08CE        0000


V2 M10   ACTUAL  8K  CONFIG  8K

// FOR
*LIST SOURCE PROGRAM
*IOCS(TYPEWRITER,KEYBOARD,DISK,CARD,1132PRINTER,PLOTTER)
C ********************************************************************
C *    SOLUTION OF TWO PARTIAL DIFFERENTIAL EQUATIONS                *
C *    BY THE 4TH ORDER RUNGE-KUTTA METHOD                           *
C ********************************************************************
      DIMENSION X(2,10),XO(2,10)
      DIMENSION X1(20),Y1(20)
      DIMENSION XTITL(5),YTITL(5)
      READ (2,8) TMAX,DELT
      READ (2,80) R1,R2,SV
      READ(2,81) EPS,V
      READ(2,82)CF,CSAT
      READ(2,83)  JN,XL
      READ(2,60) JJMAX
      READ (2,50) (XTITL(K),K=1,5)
      READ(2,51) (YTITL(K), K=1,5)
8     FORMAT (F10.2,F10.2)
80    FORMAT(F10.7,F10.7,E15.5)
81    FORMAT(F10.5,F10.5)
82    FORMAT(F10.5,F10.5)
83    FORMAT(I10,F10.5)
60    FORMAT (I10)
50    FORMAT (5A4)
51 *  FORMAT (5A4)
      DZ=1./FLOAT(JN-1)
      DDZ=XL/FLOAT(JN-1)
      WRITE(3,90)
90    FORMAT(1H1,74HSOLUTION OF PARTIAL DIFFERENTIAL EQUATIONS BY 4TH OR
     $DER RUNGE-KUTTA METHOD)
      WRITE(3,91)
91    FORMAT(1X,74(1H*))
      WRITE(3,92)
92    FORMAT(1X,//42H THE PARAMETERS + INITIAL CONDITIONS ARE  )
      WRITE(3,93) EPS,V,R1,R2,CF
93    FORMAT(1X,21HVOID FRACTION   EPS =,F5.3,13X,18HGAS VELOCITY   V =

     $,F5.1,/1X,22HFORW'D RATE CST   R1 =,F10.7,7X,23HREVERSE RATE CST
     $ R2 =,F10.7,/1X,29HGAS FEED CONCENTRATION   CF =,F7.5)
      WRITE(3,99) DELT,DDZ
99    FORMAT(1X,10HTIME INCR.,F10.5,19X,11HSPACE INCR.,F10.5)
      WRITE(3,70) TMAX,XL
70    FORMAT(1X,28HDURATION OF THE EXP'T TMAX =,F9.3 ,2X,22HHEIGHT OF TH
     $E BED XL =,F10.7)
      WRITE (3,75)
75    FORMAT(1HO,5X,26HALL UNITS IN THE SI SYSTEM)
      T=0.
      WRITE (3,13) T
```

```
      DO 100 J=1,JN
      XO(1,J)=0.
      XO(2,J)=1.
      X(1,J)=0.
      X(2,J)=0.
      WRITE (3,12) XO(1,J),XO(2,J)
12    FORMAT(10X,7HTHETA =,E15.4,5X,5HPSI =,E15.4)
100   CONTINUE
      KK=1
      X1(KK)=0.
      Y1(KK)=0.
      H=DELT/TMAX
      B1=TMAX*SV*R1*CF/(CSAT*(1.-EPS)*3600.)
      B2=SV*R2*TMAX/(CSAT*(1.-EPS)*3600.)
      B3=TMAX*V/(XL*EPS)
      B4=SV*R1*TMAX*(1.-EPS)/EPS
      B5=TMAX*SV*R2*(1.-EPS)/(EPS*CF)
175   JJ=0
300   JJ=JJ+1
      T=T+DELT
      Z=0.
      I=JN-1
      X(1,1)=XO(1,1)+H*(B1*XO(2,1)*(1.-XO(1,1))-B2*XO(1,1))
      X(2,1)=1.
      DO 101 J=2,I
      AK1=H*(B1*XO(2,J)*(1.-XO(1,J))-B2*XO(1,J))
      AL1=H*(B3*(XO(2,J-1)-XO(2,J+1))/(2.*DZ)-B4*XO(2,J)*(1.-XO(1,J))
     $+B5*XO(1,J))
      AK2=H*(B1*(XO(2,J)+AL1/2.)*(1.-XO(1,J)-AK1/2.)-B2*(XO(1,J)+AK1/2.
     $))
      AL2=H*(B3*(XO(2,J-1)-XO(2,J+1))/(2.*DZ)-B4*(XO(2,J)+AL1/2.)*(1.-
     $XO(1,J)-AK1/2.)+B5*(XO(1,J)+AK1/2.))
      AK3=H*(B1*(XO(2,J)+AL2/2.)*(1.-XO(1,J)-AK2/2.)-B2*(XO(1,J)+AK2/2.
     $))
      AL3=H*(B3*(XO(2,J-1)-XO(2,J+1))/(2.*DZ)-B4*(XO(2,J)+AL2/2.)*(1.-XO
     $(1,J)-AK2/2.)+B5*(XO(1,J)+AK2/2.))
      AK4=H*(B1*(XO(2,J)+AL3)*(1.-XO(1,J)-AK3)-B2*(XO(1,J)+AK3))
      AL4=H*(B3*(XO(2,J-1)-XO(2,J+1))/(2.*DZ)-B4*(XO(2,J)+AL3)*(1.-XO(1
     $,J)-AK3)+B5*(XO(1,J)+AK3))
      X(1,J)=XO(1,J)+(AK1+2.*AK2+2.*AK3+AK4)/6.
      X(2,J)=XO(2,J)+(AL1+2.*AL2+2.*AL3+AL4)/6.
101   CONTINUE
      X(1,JN)=XO(1,JN)+AK1
      X(2,JN)=XO(2,JN)+H*(B3*(XO(2,JN-1)-XO(2,JN))/DZ-B4*XO(2,JN)*(1.-XO
     $(1,JN))+B5*XO(1,JN))
      DO 102 J=1,JN
      XO(1,J)=X(1,J)
      XO(2,J)=X(2,J)
102   CONTINUE
      IF(T-TMAX) 180,400,400
180   Z=0.
      IF(JJ-JJMAX) 300,250,250
250   WRITE (3,13) T
13    FORMAT(2X,//19H SITUATION AT TIME=,F10.3)
      WRITE(3,14)
14    FORMAT(15X,1HZ,15X,5HTHETA,15X,3HPSI)
      KK=KK+1
      X1(KK)=T/TMAX
      A=0.
```

```
PAGE    3

      DO 450 J=1,JN
      A=A+X(1,J)
450   CONTINUE
      Y1(KK)=A/FLOAT(JN)
      DO 103 J=1,JN
      WRITE(3,20) Z,X(1,J),X(2,J)
20    FORMAT (10X,3(E15.4,5X))
      Z=Z+DDZ
103   CONTINUE
      GO TO 175
400   CONTINUE
      WRITE (3,30)
30    FORMAT(//20X,22HSOLUTION TIME EXCEEDED)
      CALL LINSG(2,2,0.0,0.0,0.0,0.0,1.0,1.0,0,XTITL,YTITL)
      CALL PUTPT(0,0,0.0,0.0,0.0,0.0,1.0,1.0,0,X1,Y1,17)
      CALL PDRAW(0,0,0.0,0.0,0.0,0.0,1.0,1.0,X1,Y1,17)
      CALL PSKIP
      STOP
      END

FEATURES SUPPORTED
 IOCS

CORE REQUIREMENTS FOR
 COMMON       0  VARIABLES    272  PROGRAM   1486

RELATIVE EXECUTION ADDRESS IS 0253 (HEX)

 END OF COMPILATION

// XEQ           1

*LOCAL,PUTPT,PDRAW,PSKIP,LINSQ,KEYSQ
```

SOLUTION OF PARTIAL DIFFERENTIAL EQUATIONS BY 4TH ORDER RUNGE-KUTTA METHOD

THE PARAMETERS + INITIAL CONDITIONS ARE

VOID FRACTION EPS =0.650 GAS VELOCITY V = 0.1

FORW'D RATE CST R1 = 0.0400000 REVERSE RATE CST R2 = 0.0000002

GAS FEED CONCENTRATION CF =1.00000

TIME INCR. 0.00100 SPACE INCR. 0.00125

DURATION OF THE EXP'T TMAX = 8.000 HEIGHT OF THE BED XL = 0.0050000

ALL UNITS IN THE SI SYSTEM, EXCEPT TIME IN HOURS

SITUATION AT TIME= 0.000

THETA =	0.0000E 00	PSI =	1.0000E 00
THETA =	0.0000E 00	PSI =	1.0000E 00
THETA =	0.0000E 00	PSI =	1.0000E 00
THETA =	0.0000E 00	PSI =	1.0000E 00
THETA =	0.0000E 00	PSI =	1.0000E 00

SITUATION AT TIME= 0.499

Z	THETA	PSI
0.0000E 00	6.2658E-01	1.0000E 00
1.2500E-03	2.5366E-01	3.3499E-01
2.5000E-03	8.0078E-02	9.3186E-02
3.7500E-03	2.6462E-02	2.3926E-02
4.9999E-03	2.7466E-02	8.6560E-03

SITUATION AT TIME= 0.999

Z	THETA	PSI
0.0000E 00	8.6054E-01	1.0000E 00
1.2500E-03	4.9346E-01	4.6516E-01
2.5000E-03	1.7869E-01	1.4322E-01
3.7500E-03	5.4727E-02	3.7660E-02
4.9999E-03	5.5719E-02	1.3871E-02

SITUATION AT TIME= 1.499

Z	THETA	PSI
0.0000E 00	9.4790E-01	1.0000E 00
1.2500E-03	7.1171E-01	7.0530E-01
2.5000E-03	3.1969E-01	2.5614E-01
3.7500E-03	1.0131E-01	7.0141E-02
4.9999E-03	1.0227E-01	2.6631E-02

SITUATION AT TIME= 1.999

Z	THETA	PSI
0.0000E 00	9.8052E-01	1.0000E 00
1.2500E-03	8.7933E-01	1.0652E 00
2.5000E-03	5.2936E-01	5.2745E-01
3.7500E-03	1.9108E-01	1.5724E-01
4.9999E-03	1.9198E-01	6.3571E-02

SITUATION AT TIME= 2.499

Z	THETA	PSI
0.0000E 00	9.9270E-01	1.0000E 00
1.2500E-03	9.5935E-01	1.0369E 00
2.5000E-03	7.6525E-01	8.5599E-01
3.7500E-03	3.5518E-01	3.0513E-01
4.9999E-03	3.5601E-01	1.4041E-01

SITUATION AT TIME= 2.999

Z	THETA	PSI
0.0000E 00	9.9725E-01	1.0000E 00
1.2500E-03	9.8303E-01	7.6931E-01
2.5000E-03	9.0507E-01	9.5717E-01
3.7500E-03	5.5323E-01	4.3996E-01
4.9999E-03	5.5406E-01	2.4263E-01

SITUATION AT TIME= 3.499

Z	THETA	PSI
0.0000E 00	9.9895E-01	1.0000E 00
1.2500E-03	9.9168E-01	7.2089E-01
2.5000E-03	9.6341E-01	9.7724E-01
3.7500E-03	7.3041E-01	5.9143E-01
4.9999E-03	7.3126E-01	3.9633E-01

SITUATION AT TIME= 3.999

Z	THETA	PSI
0.0000E 00	9.9958E-01	1.0000E 00
1.2500E-03	9.9603E-01	8.0524E-01
2.5000E-03	9.8605E-01	9.8559E-01
3.7500E-03	8.6113E-01	7.5539E-01
4.9999E-03	8.6205E-01	6.0227E-01

SITUATION AT TIME= 4.499

Z	THETA	PSI
0.0000E 00	9.9982E-01	1.0000E 00
1.2500E-03	9.9826E-01	9.0118E-01
2.5000E-03	9.9470E-01	9.9227E-01
3.7500E-03	9.3823E-01	8.8207E-01
4.9999E-03	9.3920E-01	7.9280E-01

SITUATION AT TIME= 4.999

Z	THETA	PSI
0.0000E 00	9.9990E-01	1.0000E 00
1.2500E-03	9.9929E-01	9.5739E-01
2.5000E-03	9.9799E-01	9.9653E-01
3.7500E-03	9.7501E-01	9.5009E-01
4.9999E-03	9.7601E-01	9.0956E-01

SITUATION AT TIME= 5.498

Z	THETA	PSI
0.0000E 00	9.9993E-01	1.0000E 00
1.2500E-03	9.9970E-01	9.8220E-01
2.5000E-03	9.9922E-01	9.9855E-01
3.7500E-03	9.9032E-01	9.7939E-01
4.9999E-03	9.9134E-01	9.6386E-01

SITUATION AT TIME= 5.998

Z	THETA	PSI
0.0000E 00	9.9993E-01	1.0000E 00
1.2500E-03	9.9986E-01	9.9205E-01
2.5000E-03	9.9968E-01	9.9937E-01
3.7500E-03	9.9631E-01	9.9092E-01
4.9999E-03	9.9733E-01	9.8600E-01

SITUATION AT TIME= 6.498

Z	THETA	PSI
0.0000E 00	9.9993E-01	1.0000E 00
1.2500E-03	9.9992E-01	9.9582E-01
2.5000E-03	9.9986E-01	9.9969E-01
3.7500E-03	9.9859E-01	9.9532E-01
4.9999E-03	9.9961E-01	9.9457E-01

SITUATION AT TIME= 6.998

Z	THETA	PSI
0.0000E 00	9.9993E-01	1.0000E 00
1.2500E-03	9.9993E-01	9.9720E-01
2.5000E-03	9.9992E-01	9.9975E-01
3.7500E-03	9.9944E-01	9.9696E-01
4.9999E-03	1.0004E 00	9.9776E-01

SITUATION AT TIME= 7.497

Z	THETA	PSI
0.0000E 00	9.9993E-01	1.0000E 00
1.2500E-03	9.9993E-01	9.9781E-01
2.5000E-03	9.9993E-01	9.9976E-01
3.7500E-03	9.9977E-01	9.9759E-01
4.9999E-03	1.0007E 00	9.9894E-01

SITUATION AT TIME= 7.997

Z	THETA	PSI
0.0000E 00	9.9993E-01	1.0000E 00
1.2500E-03	9.9993E-01	9.9808E-01
2.5000E-03	9.9993E-01	9.9977E-01
3.7500E-03	9.9986E-01	9.9786E-01
4.9999E-03	1.0008E 00	9.9938E-01

SOLUTION TIME EXCEEDED

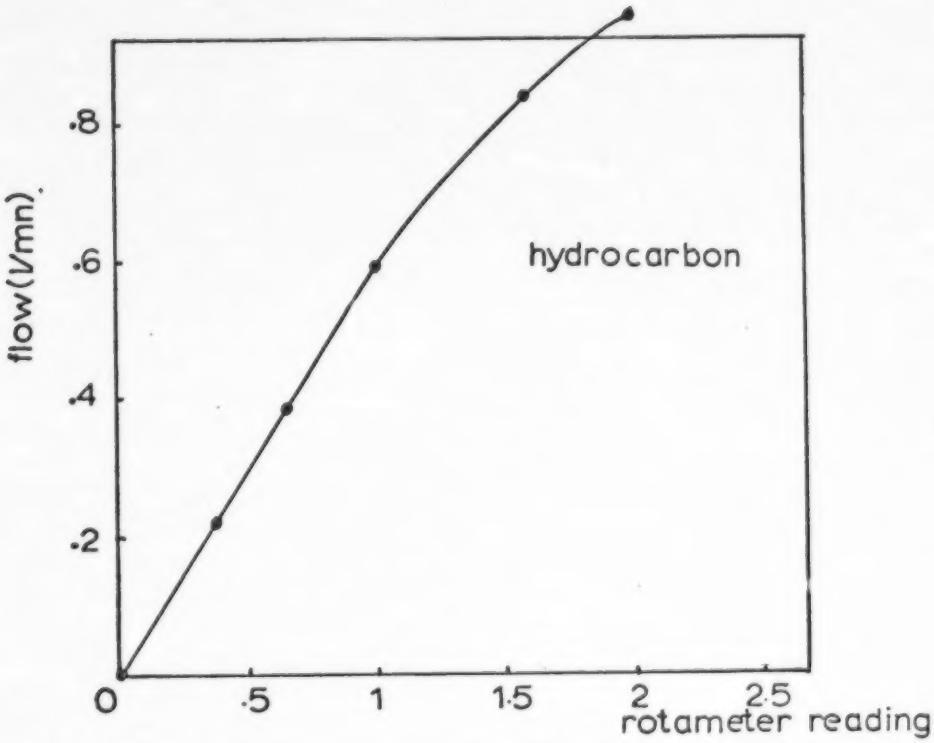

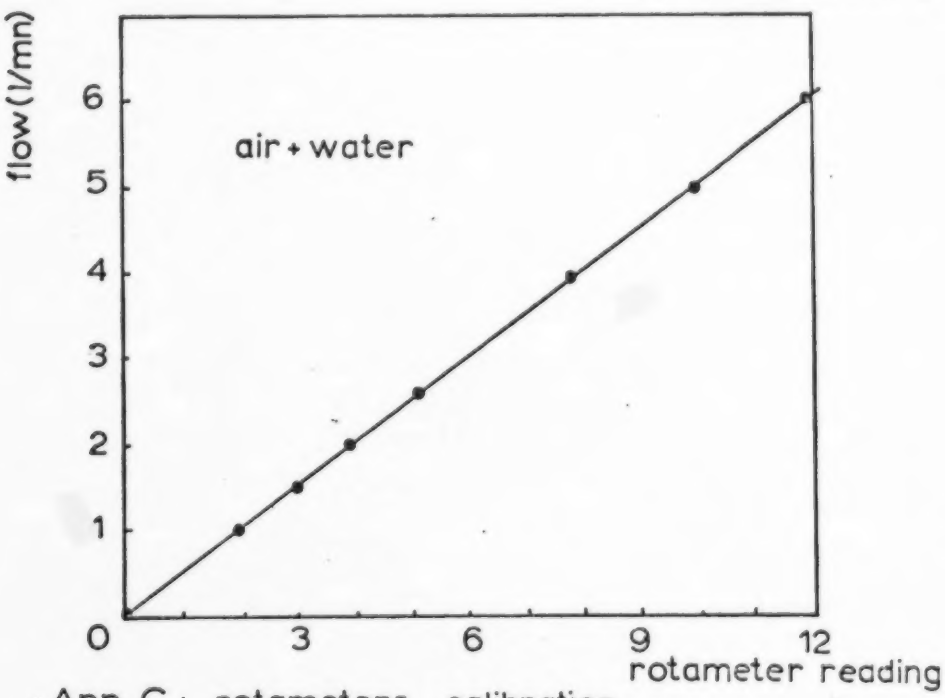

App. C : rotameters calibration